CZECH TECHNICAL UNIVERSITY IN PRAGUE

FACULTY OF MECHANICAL ENGINEERING

DEPARTMENT OF AUTOMOTIVE, COMBUSTION ENGINE AND RAILWAY ENGINEERING

MASTER THESIS

Cooling and Heat Exchangers for Hydrogen Fuel Cell System

Author: Ogul Can Güngör

Supervisor: prof. Ing. Jan Macek, DrSc.

Program: Master of Automotive Engineering

Specialization: Advanced Powertrain Design

August 2020

MASTER'S THESIS ASSIGNMENT

I. Personal and study details

Student's name: **Güngör Ogul Can** Personal ID number: **472895**

Faculty / Institute: **Faculty of Mechanical Engineering**

Department / Institute: **Department of Automotive, Combustion Engine and Railway Engineering**

Study program: **Master of Automotive Engineering**

Branch of study: **Advanced Powertrains**

II. Master's thesis details

Master's thesis title in English:

Cooling and Heat Exchangers for Hydrogen Fuel Cell System

Master's thesis title in Czech:

Chlazení a výměníky tepla pro systém vodíkového palivového článku

Guidelines:

Elaborate the following items as the base for the future radiator system optimization:
1. Describe fuel cell system and its necessary components.
2. Investigate possible solutions for cooling and heat accumulation of the fuel cell system.
3. Calculate necessary cooling surface (radiator size) for selected radiator lay-outs based on different FC load profiles and boundary conditions.
4. Design new space optimized cooling system for DEVINN hydrogen fuel cell system.
5. Assess the cooling power of designed radiator

Bibliography / sources:

[1] Adam Z. Weber and John Newman, Modeling Transport in Polymer-Electrolyte Fuel Cells. Chem. Rev. 2004, 104, 4679-4726
[2] A. A. Kulikovsky, Quasi-3D Modeling of Water Transport in Polymer Electrolyte Fuel Cells. Journal of The Electrochemical Society, 150 (11) A1432-A1439, 2003. DOI: [10.1149/1.1611489]
[3] Benedikt Hollweck, Thomas Korb, Gregor Kolls, Timo Neuner, Jörg Wind, Analyses of the holistic energy balance of different fuel cell powertrains under realistic boundary conditions and user behaviours. WHTC Congress Prague 2017, prepare for publication in Journal of Hydrogen Technology, Elesevier
[4] Manual and On-line Help for GT Suite Code, Beta version 2020, Gamma Technologies 2020, www.gtisoft.com
[5] Macek J. et al., FC PEM Model for Compressor Assignment and Overall Optimization. Internal report CVUT-FS, U 12021 Z19-20, Prague 2020

Name and workplace of master's thesis supervisor:

prof. Ing. Jan Macek, DrSc., Department of Automotive, Combustion Engine and Railway Engineering, FME

Name and workplace of second master's thesis supervisor or consultant:

Ing. Jiří Vršínský, DEVINN s.r.o.

Date of master's thesis assignment: **09.03.2020** Deadline for master's thesis submission: **14.08.2020**

Assignment valid until: _____

prof. Ing. Jan Macek, DrSc.	doc. Ing. Oldřich Vítek, Ph.D.	prof. Ing. Michael Valášek, DrSc.
Supervisor's signature	Head of department's signature	Dean's signature

Declaration

I, Ogul Can Güngör, declare that this thesis and the work presented in it, titled “Cooling and Heat Exchangers for Hydrogen Fuel Cell System”, are my own and has been generated by me as the result of my own original research. I confirm that this work was done wholly or mainly while in candidature for master’s degree in Automotive Engineering at Czech Technical University. Where any part of this thesis has previously been submitted for a degree or any other qualification at this University or any other institution, this has been clearly stated. Where I have consulted the published work of others, this is always clearly attributed. Where I have quoted from the work of others, the source is always given. With the exception of such quotations, this thesis is entirely my own work. I have acknowledged all main sources of help. None of this work has been published before submission.

Date: Thursday, August 13, 2020 Signature:

Acknowledgments

I would first like to express my gratitude to my supervisor, prof. Ing. Jan Macek, DrSc., for his support and guidance. I am very grateful for his directions which helped me to write my thesis.

I would also like to sincerely thank DEVINN s.r.o. and Ing. Jiří Vršínský for the trust they put in me. Whenever I had a problem to solve, Mr. Vršínský's door was always open to me.

Last but not least, my special thanks also belong to my family, for their continuous encouragement, unfailing support and endless love.

Abstrakt

V této diplomové práci je představen návrh chladicího systému a tepelného výměníku pro odul palivových buňek. Cílem diplomové práce je navrhnout tepelný výměník spolu s dalšími součástmi chladicího systému, jaké jsou ventilátor a čerpadlo, tak aby byly v souladu s počátečními podmínkami. Obsahem této práce jsou též typy palivových buněk, modul palivových buněk, jeho nezbytné součásti a řešení pro chlazení modulu palivových buněk. Na základě stanovených podmínek byly navrženy dva tepelné výměníky s různými designy, byla vysvětlena jejich teorie a metodologie, též byly vybrány ventilátor a čerpadlo pro oba designy.

Klíčová slova

Chladič automobilového typu, tepelný výměník, kompaktní tepelný výměník, palivový článek s protonově propustnou membránou, chladicí systém, ventilátor, čerpadlo chladicí tekutiny

Abstract

In this master's thesis study, cooling system and heat exchanger design for of a fuel cell module is presented. The aim of the prepared thesis is to design heat exchanger along with other cooling system components, being fan and pump, in accordance with initial conditions. Content of this study consists also of fuel cell types, fuel cell module, its necessary components and solution for cooling of the fuel cell module. According to the given conditions, two heat exchangers with different layouts have been designed and theory and methodology behind it has been discussed, as well as fan and pump for both designs has been selected.

Keywords

Radiator, heat exchanger, compact heat exchanger, fuel cell, cooling system, fan, pump

Nomenclature

Symbols

A	$Area, [m^2]$
c	$Specific\ heat\ capacity, [J/kgK]$
C	$Total\ heat\ capacity, [W/K]$
D	$Diameter, [m]$
G	$Mass\ flux, [kg/m^2s]$
h	$Heat\ transfer\ coefficient, [W/m^2K]$
H	$Height, enthalpy\ [m, J]$
K	$Coefficient, [-]$
L	$Length, [m]$
m	$mass, [kg]$
p	$Pressure, [Pa]$
P	$Power, [W]$
R	$Resistance, [K/W]$
Q	$Heat\ transfer, [W]$
T	$Temperature, [°C, K]$
u	$Velocity, [m/s]$
W	$Width, [m]$

Greek letters

ε	$Effectiveness, [-]$
ρ	$Density, [kg/m^3]$
η	$Efficiency, [-]$
μ	$Dynamic\ viscosity, [Pas]$
ν	$Kinematic\ vistosity, [m^2/s]$

Subscripts

a	Air
al	$Aluminum$
ch	$Channel$
cu	$Copper$
e	$Exit$
f	$Fin, finned, fouling$
ff	$Free\ flow$
gen	$Generated$
i	$Inlet, inner$
o	$Outlet, outer$
p	$Constant\ pressure$
t	$Tube$
uf	$Unfinned$
r	$Radiator$
v	$Constant\ volume$
w	$Water$

Abbreviations

CF	$Correction\ factor$
CHE	$Compact\ heat\ exchanger$
HE	$Heat\ exchanger$
HTC	$Heat\ transfer\ coefficient$
$LMTD$	$Log\ mean\ temperature\ differ$
NTU	$Number\ of\ transfer\ units$

Contents

Abstrakt 5
Klíčová slova 5
Nomenclature 6
1. Introduction 10
2. Fuel Cell Fundamentals and Necessary Components 10
2.1. Fuel Cell 11
2.2. Working Principle 12
2.3. Types of Fuel Cell 14
2.3.1. Proton Exchange Membrane Fuel Cell (PEMFC) 14
2.3.2. Phosphoric Acid Fuel Cell (PAFC) 15
2.3.3. Solid Oxide Fuel Cell (SOFC) 16
2.3.4. Molten Carbonate Fuel Cell (MCFC) 17
2.3.5. Alkaline Fuel Cell (AFC) 19
2.3.6. Comparison of FC Types 20
2.4. Components of a Fuel Cell 21
2.4.1. Membrane 22
2.4.2. Catalyst Layers 22
2.4.3. Gas Diffusion Layer (GDL) 24
2.4.4. Bipolar Plates 24
2.4.5. Gasket 25
2.4.6. Current Collecting Plates 25
2.5. Fuel Cell Module 25
2.5.1. Compressor 26
2.5.2. Pump 27
2.5.3. Ion Exchange Filter 27
2.5.4. Battery 27
2.5.5. DC/DC Inverter 28
2.5.6. Control Unit 28
3. Cooling and Heat Accumulation of the FC system 28
3.1. Cooling Strategies 29
3.2. Heat Management of Fuel Cells 32
3.2.1. Fuel Cell Energy Balance 32
3.3. Heat Exchangers for Fuel Cells 33
3.3.1. Heat Exchanger Modelling 34

4. Methodology and Results 35
4.1. Design N^o 1 37
4.1.1. Sensitivity Analysis 45
4.2. Design N^o 2 48
4.2.1. Sensitivity Analysis 54
4.3. Fan 57
4.4. Pump 59
4.5. Cooling Power 60
5. Conclusion 61
References 62
APPENDIX 65

List of Figures

Figure 1: Fuel Cell diagram [4] 12
Figure 2: FC schematic 13
Figure 3: PEMFC schematic [7] 14
Figure 4: SOFC schematic [7] 17
Figure 5: MCFC schematic [7] 18
Figure 6: AFC schematic [7] 19
Figure 7: Parts of a PEMFC 22
Figure 8: Catalyst layer and GDL structure 23
Figure 9: DEVINN s.r.o. Fuel Cell module scheme 26
Figure 10: DEVINN battery pack 28
Figure 11: FC module coolant system 29
Figure 12: Cooling strategies 29
Figure 13: System layout of cooling with liquid [20] 31
Figure 14: System layout of evaporative cooling 32
Figure 15: FC energy balance scheme 33
Figure 16: Space requirement for the radiator 36
Figure 17: Schematic of radiator #1 37
Figure 18: Mass flow rate effect 45
Figure 19: Specific heat capacity effect 45
Figure 20: Cr when air flow is constant 46
Figure 21: Cr when water flow is constant 46
Figure 22: Air outlet temperature effect 47
Figure 23: Rea effect 47
Figure 24: Effect of radiator height 47
Figure 25: Effect of radiator area 47
Figure 26: Schematic of radiator #2 48
Figure 27: Effect of mass flow rate 54
Figure 28: Effect of specific heat capacity 54
Figure 29: Cr when air flow is constant 55
Figure 30: Cr when water flow is constant 55
Figure 31: Air outlet temperature 56

Figure 32: Effect of Rea 56
Figure 33: Effect of radiator height 56
Figure 34: Effect of radiator area 56
Figure 35: Brushless VA113-BBL504P/N-94A 58
Figure 36: Brushless VA89-BBL338P/N-94A 59

List of Tables

Table 1: Comparison and summary of FC types 20
Table 2: DEVINN FC module battery properties 27
Table 3: Possible solutions for cooling of PEMFC [19] 30
Table 4: Initial conditions 35
Table 5: Input parameters for design #1 37
Table 6: Water thermal properties from Incropera 38
Table 7: Air thermal properties from Incropera 38
Table 8: Area calculation results 39
Table 9: Obtained results 41
Table 10: Major results 43
Table 11: Pressure drop values 44
Table 12: Input parameters for design #2 49
Table 13: Water thermal properties from Shah 49
Table 14: Air thermal properties from Shah 49
Table 15: Obtained results 51
Table 16: Major results 53
Table 17: Pressure drop values 54
Table 18: Fan selection for the first radiator 57
Table 19: Fan selection for the second radiator 58
Table 20: Pump selection for both radiators 59
Table 21: Cooling power 61

1. Introduction

In today's technology, hydrogen fuel cells offer numerous advantages in comparison to power sources in established usage i.e. combustion engines in vehicles. Fuel cells do not burn oil or gas since they are powered by hydrogen or methane. Fuel cells with green hydrogen significantly reduce pollution which is essential in terms of emissions legislations and air quality. The biggest emission of them is water. Hydrogen fuel cells are more efficient when compared to petrol engines as they can obtain more energy in Joules out of the fuel [1]. They are also advantageous for longer ranges of driving and short amount of charging in case of battery electric vehicle applications. A fuel cell operated vehicle with a full tank will give roughly 450 kilometers of range and similar to combustion engine tanks, hydrogen tank can be refilled with pressurized hydrogen in several minutes.

There are many types of fuel cells depending on what type of electrolyte or membrane is being used and that depends on if the fuel cells operate at low or high temperature. Each type of fuel cell has different areas of usage and has its own advantages and disadvantages which will be discussed later on in this paper.

Fuel cells mostly need to overcome the environmental changes i.e. temperature, vibration etc. in order to sustain cooling homogeneity. There are several ways to achieve successful cooling. In case of fuel cells which operate at low temperatures, there is a need for a heat exchanger and that is because once high environment temperature is reached, rejecting the low temperature heat is difficult. Emitted water is evaporated with absorption of the heat at cathode side. Nevertheless, heat can be transferred to radiator with an air or liquid cooled cooling system so that the heat can be rejected.

Considering the advantages of the fuel cells and existing and upcoming solutions for the possible issues, hydrogen fuel cells offer significant benefits in terms of efficiency, pollutant reduction, performance and reliability. [2]

2. Fuel Cell Fundamentals and Necessary Components

In this part, fuel cells (FCs) will be described and its classification with brief explanations will be delivered. Afterwards, operation principles of FCs and its essential components will be explained.

2.1.Fuel Cell

FCs, nowadays, have a wider range of applications and areas of usage when compared to first years of its discovery as being a new energy generation technology that is efficient, quiet and environment friendly. FCs are power elements that convert the chemical energy of the input fuel into usable energy in the form of direct current (DC) electricity and heat, without a combustion and without using any intermediate element or reaction. In other words, FC is a device which converts energy by reaction of hydrogen or methane with oxygen that enter into it and having electricity, heat and water as products of the reaction (See Figure 1).

Although the fuel cell working principle was discovered in 1889, it was not used in power generation until the 1960s space programs. Fuel cell technology has improved significantly in recent years with the support of states and private sectors. FCs have since made their way in several various applications. The high-power and efficiency make the system ideal for the transport industry since zero emission vehicles become more attractive [3].

Conventional power systems are non-renewable and require combustion to generate power. However, fuel cell systems do not require combustion and are also different from conventional power systems in terms of not having rotating parts. FCs have following advantages over the conventional ones:

- Energy production efficiency is high.
- Green hydrogen FCs have low environmental effects such as low greenhouse gas emission, being silent and solid waste free.
- The operating characteristic provides ease in application.
- They can work with different types of fuel source.
- FC powered vehicles bring almost instant recharging opportunity.

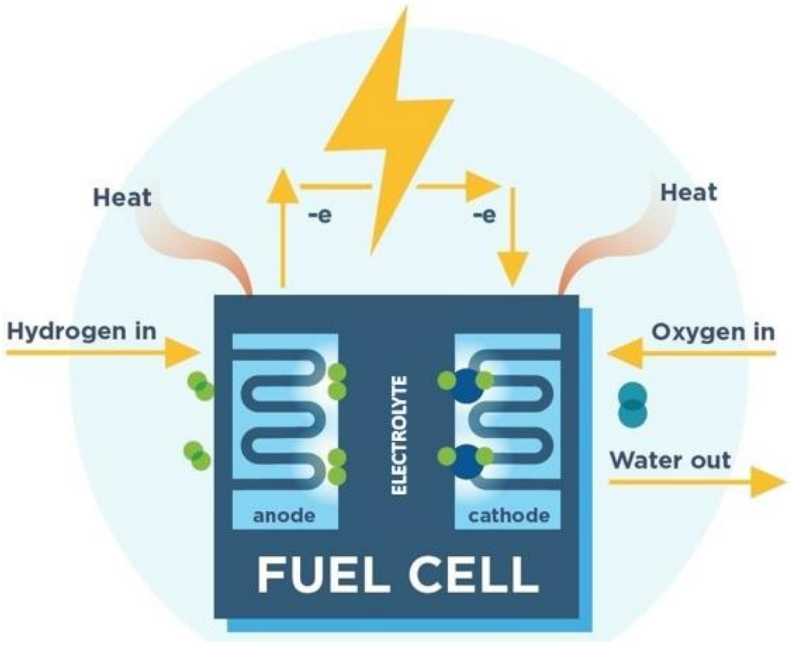

Figure 1: Fuel Cell diagram [4]

On the other hand, following restrictions can be stated for almost every FC system:

- Depending on which type of fuel is being used, catalytic process might be needed so that the fuel can react at lower temperatures.
- When a fuel, which is not as pure as green hydrogen, is used, efficiency of FC becomes lower by time due to possible catalyst and electrolyte failure. [2]
- In case product water evaporates very fast or very slow, FC may get damaged due to overheating or electrodes may lose its function which in return stops the chemical reaction [5].

2.2. Working Principle

FCs basically combine the fuel of hydrogen with air and react with this reaction, resulting in electricity, heat and water. The FC is supplied with hydrogen fuel from the anode and air from the cathode. Hydrogen decomposes to positive and negative ions on the anode side. Positive ions pass through the electrolyte, which only allows the passage of positively charged ions, reaching the cathode tip. The electrons remaining at the anode end tend to recombine with positively charged ions and flow to the cathode side with an external circuit. Following this electron flow in the external circuit, electricity is produced. Electrons crossing the cathode side combine with positive ions and air to produce pure water. The reactions of this process are as follows below.

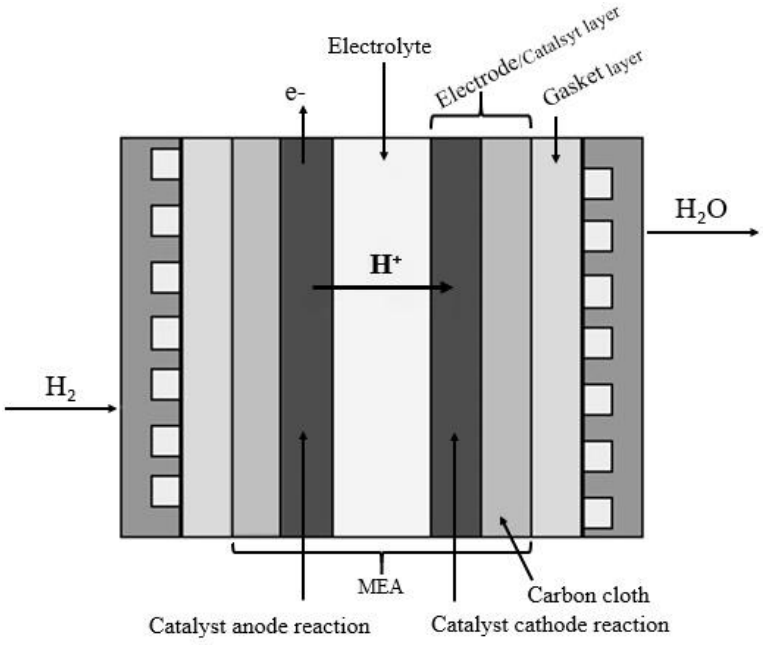

Figure 2: FC schematic

$$Anode\ reaction: H_2 \rightarrow 2H^+ + 2e^-$$

$$Cathode\ reaction: {}^1/_2\, O_2 + 2H^+ + 2e^- \rightarrow H_2O$$

$$Total\ reacion: H_2 + {}^1/_2\, O_2 \rightarrow H_2O + electrical\ energy + heat$$

If we gradually explain electricity production with FC:

- 1st Stage: Hydrogen is added to the FC.
- 2nd Stage: The hydrogen entering the FC is decomposed into ions by catalysts on the anode surface and prevents electron transfer. Hence, only protons pass through the electrode and flow into the cathode.
- 3rd Stage: These electrons, which cannot pass through the electrolyte, also create an electric current by switching to the cathode through a conductive external circuit.
- 4th Stage: The protons passing through the cathode combine with electrons from the external circuit and form hydrogen again.
- 5th Stage: Hydrogen combines with the air supplied by the cathode to form water, and water is transferred to the outside as an exhaust.

The byproducts, H_2O and waste heat, produced by the FC may affect action of some type of FCs negatively and thus, they need to be constantly drained.

2.3. Types of Fuel Cell

The basic fuel cell structure consists of two electrodes and an electrolyte packaged between these electrodes. Fuel cells are classified according to the material used as electrolyte since it is electrolyte defining the1 working temperature.

2.3.1. Proton Exchange Membrane Fuel Cell (PEMFC)

Especially after the discovery of high-performance polymers; PEMFCs were developed to be used in space studies and special military systems. However, being able to handle higher energy densities and quickly start up, such FCs are very much desired in automotive industry either. PEMFC is the most interesting and promising type of FC due to its high efficiency at low operating temperatures, silent operation and no waste other than pure water.

The main component of PEMFC contains two electrodes, anode and cathode as it can be seen in Figure 3. These are separated from each other by a polymer membrane. Both electrodes are covered with a thin platinum catalyst layer on one side. Electrodes form the membrane electrode, together with catalyst and membrane. Hydrogen used as fuel is fed from the anode side of the FC. In the presence of platinum catalyst in the anode, it decomposes into monoatomic active hydrogen that is ionized into free electrons and protons. Free electrons are used in the outer cycle and act in the form of electric current. Protons move through the polymer membrane electrolyte to the cathode, the oxygen from the air in the cathode, electrons from the outer cycle and protons combine to form pure water and heat. Individual FCs produce about slightly less than a Volt and to generate the desired amount of electricity, FCs are combined in serial as FC stacks. [6]

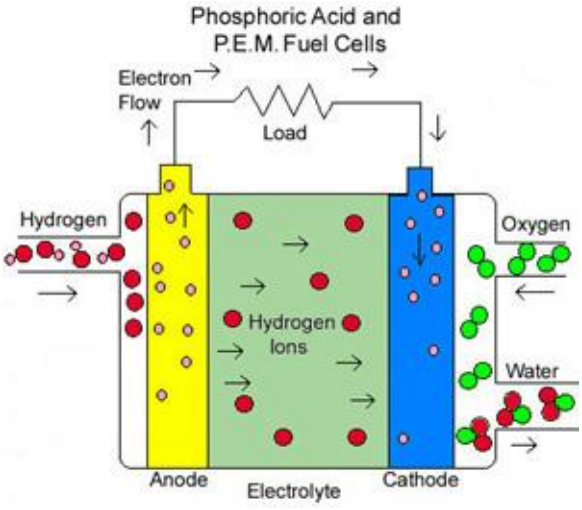

Figure 3: PEMFC schematic [7]

PEMFCs do not contain moving parts and therefore they do not result in solid friction losses, they operate very quietly and do not generate any waste. They have high efficiency about up to 60% and can operate under precise operating conditions (≈ 85 °C, 600 kPa). PEMFCs can achieve maximum efficiency at low power levels and efficiency decreases linearly with increasing power.

The chemical reaction in cathode, anode and cell during the operation of PEMFC are given below. As seen in the total reaction, the only product is water.

$$Anode\ reaction: 2H_2 \rightarrow 4H^+ + 4e^-$$

$$Cathode\ reaction: 4H^+ + 4e^- + O_2 \rightarrow 2H_2O$$

$$Total\ reaction: 2H_2 + O_2 \rightarrow 2H_2O$$

The most important element of PEMFCs is the polymeric membrane with proton conduction feature. Studies related to the development of polymeric membranes are at the top of the studies regarding FCs. Due to the low diversity and high prices of commercially used membranes today, studies on the development of alternative membranes have accelerated considerably. Membrane of PEMFC should have following characteristics:

- Proton permeability,
- No water, fuel, oxygen and other gases in the air should pass through,
- High mechanical strength, and high thermal and chemical resistances in long term use,
- It should be safe and affordable in order to be used widely in technology.

Diffusion of liquid water is very important for membrane conductivity. Membranes used in PEMFCs must be fully saturated with water in order to work with high efficiency. Studies show that when the membrane is fully saturated, high ionic conductivity is achieved.

2.3.2. Phosphoric Acid Fuel Cell (PAFC)

The PAFC consists of anode and cathode made of carbon paper containing carbon black to hold platinum catalyst particles. For a descriptive visual of this FCs as well, Figure 3 can be referred. Electrolyte is liquid phosphoric acid (H_3PO_4) and operating temperature ranges from 150°C to 220°C. H_3PO_4 has very good ionic conductivity and very good durability. However, H_3PO_4 below 150°C has poor ionic conductivity, while H_3PO_4 above 220°C is not resistant. Platinum catalyst at the anode and cathode is desired to increase the chemical reaction at the

operating temperature of PAFC. PAFC electrodes have a recyclable layer of waterproof carbon paper [8]. Such FCs have efficiency about 35-45%.

Direct hydrogen or hydrogen produced by the fuel processing unit can be used in PAFC. If the fuel processing unit is used, the CO must be removed. Because platinum catalyst can tolerate 1±0.5% of CO in fuel when working at temperatures above 150°C. H_2S and COS are collected on the platinum surface.

Active zones required for the oxidation of hydrogen are closed. Anode exhaust gas is burned to provide the necessary heat input for the fuel processing unit.

$$Anode\ reaction: H_2 \rightarrow 2H^+ + 2e^-$$

$$Cathode\ reaction: {}^1/_2\, O_2 + 2H^+ + 2e^- \rightarrow 2H_2O$$

$$Total\ reaction: H_2 + {}^1/_2\, O_2 \rightarrow H_2O$$

While the high operating temperature affects the PAFC operation, long operating time is desired to achieve the desired operating temperature. In order to maintain the desired FC stack temperature, heat management is carried out in the stack by liquid or cooling air flowing through the cooling channels. Wear is a problem for PAFC. Each battery has to work under less than a Volt to prevent the wear of carbon and platinum parts inside the PAFC. [8]

Since H_3PO_4 has sufficient ionic conductivity at the working temperature of PAFC, water management is not a problem. In order for PAFC systems to compete economically with other power generation methods, it is necessary to increase the power density of PAFC systems and to reduce costs. Another essential point is to develop abrasion resistant materials that can withstand high voltages, which are important for reducing the need for catalyst and reducing bipolar plate costs. [8]

2.3.3. Solid Oxide Fuel Cell (SOFC)

SOFC is completely solid and uses an oxide ion conductive ceramic structure as electrolyte. For this reason, it is simpler than all other defined FCs and contains only two phases of solid and gas. Expensive metal catalysts are not needed due to the high operating temperature. Both hydrogen and CO can be used as fuel. Cell reactions occur as follows:

$$Anode\ reaction: O_2 + 4e^- \rightarrow 2O^{2-}$$

$$Cathode\ reaction: 2H_2 + 2O^{2-} \rightarrow 2H_2O + 4e^-$$

$$Total\ reaction: 2H_2 + O_2 \rightarrow 2H_2O$$

Material selection is important because the operating temperature of the SOFC is quite high. Besides being a good ion and electron conductor, there are other properties. These are the stability of the materials, the cell and the ability to work together for a long time. Except for the durability of the materials, the thermal expansion of the electrode, electrolyte and interconnections should be similar. Electrolyte and interconnections should be dense enough to prevent gas mixture and electrodes should be porous enough to carry gas. Other important features are ease of production and low cost.

SOFC (See Figure 4) is similar to MCFC, which will be discussed in the following section, in a sense that the negatively charged ion, O^{2-}, from the cathode passes through the electrolyte and comes to the anode. Thus, the aquatic product is formed in the anode.

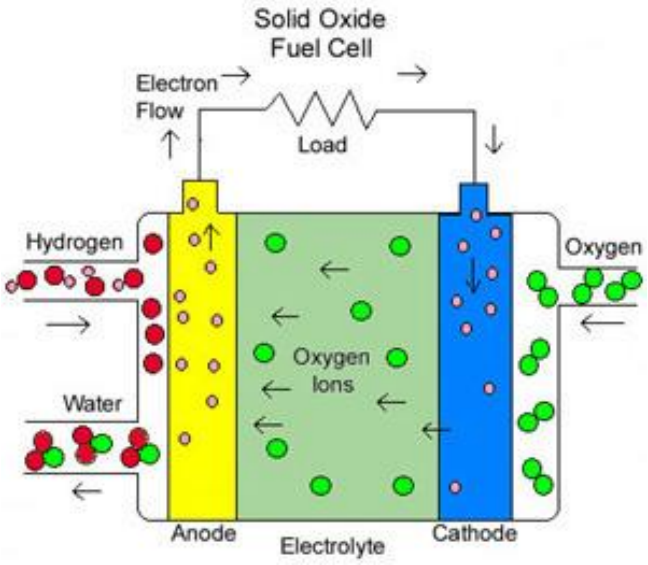

Figure 4: SOFC schematic [7]

Anode of SOFC usually consists of Zirconia ceramic, a special blend of ceramic and metal. The metallic structure is Nickel. The reason for choosing this is its high electronic conductivity and stability under chemical reduction conditions. The presence of Nickel which is partially stabilized by yttrium is translated into an advantage by using it as an internal fuel processing catalyst, and it is possible to perform internal fuel processing directly on the anode. Cathode materials are subject to great difficulties. [9]

2.3.4. Molten Carbonate Fuel Cell (MCFC)

MCFC, scheme of which is given below in Figure 5, consists of nickel alloy anode, nickel oxide cathode and $LiAlO_2$ ceramic electrolyte auxiliary matrix. The electrolyte consists of

lithium, sodium and/or potassium alkali carbonates. MCFC's operating temperature varies between 600°C and 700°C and efficiency is about 45-50%. At such temperatures, alkali carbonates are highly conductive molten salt. Nickel in anode and cathode increases chemical reactions to a sufficient level due to the high operating temperature of MCFC. Carbonate ions provide ionic conductivity.

By oxidizing hydrogen in the anode by carbonate ions; H_2O, CO_2 and electrons are produced. Electrons go from anode to cathode where O_2 and CO_2 react with electrons and produce carbonate ions in the cathode.

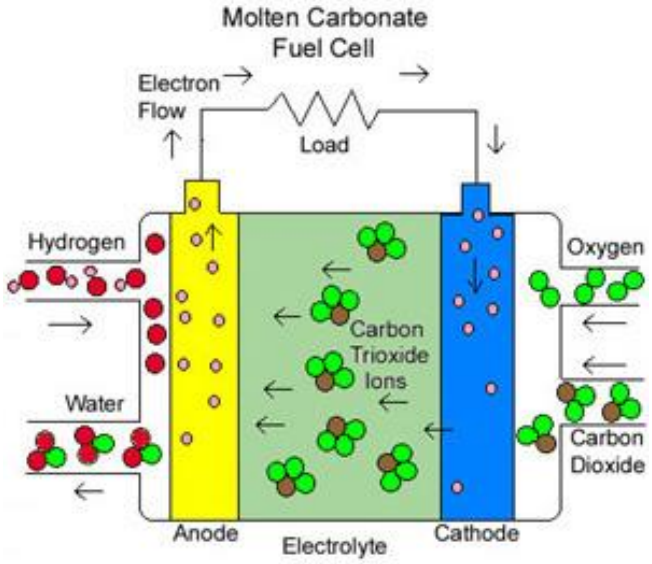

Figure 5: MCFC schematic [7]

Anode exhaust is in the form of CO_2 and water. With an external circuit, CO_2 travels to the cathode to be used during O_2 reduction. The entire reaction is exothermic and reactions that take place is as follows:

$$Anode\ reaction: H_2 + CO_3^{2-} \rightarrow CO_2 + H_2O + 2e^-$$

$$Cathode\ reaction: {}^1/_2\, O_2 + CO_2 + 2e^- \rightarrow CO_3^{2-}$$

$$Total\ reaction: H_2 + {}^1/_2\, O_2 \rightarrow 2H_2O$$

MCFC can work in wide fuel composition. The reason is it can be used in the CO fuel cell produced by the fuel processing unit since it operates at a very high temperature (i.e. 650°C) and does not use platinum catalyst. Oxidation of hydrogen at the anode occurs much faster than CO oxidation. The produced water reacts with CO with the water gas exchange reaction at the anode. This reaction produces additional hydrogen for the FC. Combustion of the anode exhaust gas provides the necessary heat input for the fuel processing unit. High temperature

operation also helps the internal steam conversion of the fuel. Internally convertible fuels in MCFC can be sorted as methane, methanol, propane and naphtha. The FC reaction provides the heat input required for the internal conversion process. Hence, the cooling requirement to balance the working temperature of the MCFC is reduced.

The disadvantages of MCFC are the high digestibility of the melted carbonate electrolyte, CO_2 requirement for cathode reaction, low sulfur tolerance, electrolyte leakage, suitable material demand at high temperatures. The advantages of MCFC are its ability to convert fuel from inside, less costly Nickel catalyst, the use of CO as fuel and its cogeneration potential. [8]

2.3.5. Alkaline Fuel Cell (AFC)

In AFC, scheme of which is given below in Figure 6, concentrated potassium hydroxide (KOH) solution is used both as a refrigerant and as an electrolyte. This solution transmits hydroxide ions from cathode to anode and operates at low temperatures around 80-100°C PEMFCs.

Due to some of its features, AFC is an alternative to PEMFC. Oxygen reduction kinetics are faster than in acid electrolytes. The voltage varies depending on the concentration of hydroxide ions accumulated in the electrolyte. Platinum and silver catalysts cause rapid separation of hydroxide ions and the potential in cathode increases. Silver can be used as a catalyst in AFCs since the alkaline medium in AFC is less corrosive than the acid medium. A cheap catalyst and a liquid electrolyte summarize the advantage of AFCs over PEMFC. Humidification of the inlet gases, which is considered as an issue in PEMFC, is not required for AFCs. [10]

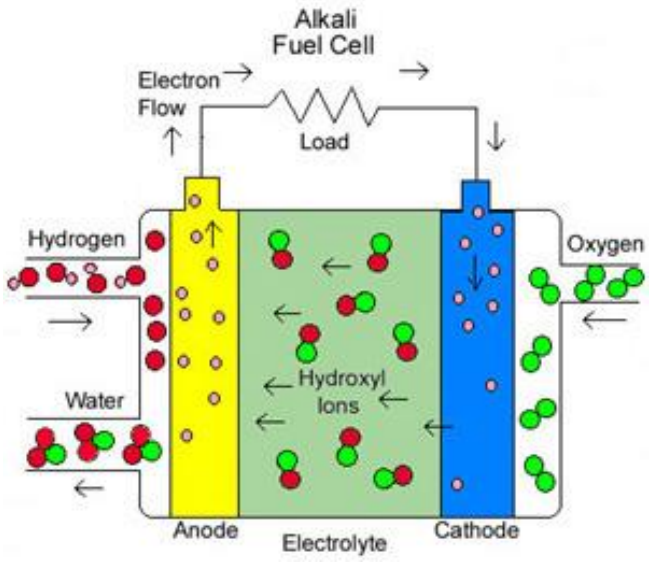

Figure 6: AFC schematic [7]

One of the drawbacks of AFC is that they are sensitive to CO^2. Fuel and oxidation medium generally contain CO^2 which reacts with the alkaline solution and produces carbonates. Resulting carbonate prevents chemical reactions in the cell. Therefore, the biggest disadvantage of AFCs is that they require very pure hydrogen. [10]

$$Anode\ reaction: 2H_2 + 4OH^- \rightarrow 4H_2O + 4e^-$$

$$Cathode\ reaction: 2H_2O + O_2 + 4e^- \rightarrow 4OH^-$$

$$Total\ reaction: 2H_2 + O_2 \rightarrow 2H_2O$$

The fact that the catalysts and pure hydrogen used are expensive and that extra energy consumption is required for liquefaction and compression of hydrogen, increases the cost of such FCs.

2.3.6. Comparison of FC Types

Having described the major FC types in the previous sections, a summarizer comparison is shown below in Table 1. [11]

Table 1: Comparison and summary of FC types

	PEMFC	**PAFC**	**SOFC**	**MCFC**	**AFC**
Electrolyte	Polymer membrane	Liquid H_3PO_4	Ion conductive ceramic structure	Liquid molten carbonates	KOH
Operating temperature	80-90 °C	150-220 °C	600-1000 °C	600-700 °C	90-100 °C
Catalyst	Platinum	Platinum	Ni/YSZ	Nickel	Platinum, silver
Transferred ion	H^+	H^+	O^{-2}	CO_3^{-2}	OH^-
Anode gas	Hydrogen	Hydrogen	Hydrogen, methane	Hydrogen, methane	Hydrogen
Cathode gas	Pure oxygen or air	Oxygen from air	Oxygen from air	Oxygen from air	Pure oxygen
Heat management	Cooler	Cogeneration	Cogeneration	Cogeneration	Cooler - Cogeneration
Efficiency	up to 60%	35-45%	45-60%	40-50%	50-70%
Applications	Transportable usage,	Relatively large power generation	Relatively large power generation	Larger power generation needs	Aerospace, military and marine

	automotive industry				
Benefits	Compact design, longer life, fast starting up	High tolerance to fuel contaminati on	High efficiency, cogeneration, fuel options	High efficiency, cogeneration, fuel options	Cheaper catalyst, liquid electrolyte
Drawbacks	Complicated heat and H_2O management , costly catalyst	Lower efficiency, cost of the catalyst	Risk of corrosion due to high temperatures, shorter life	Risk of corrosion due to high temperatures, shorter life	Sensitive to CO^2, larger in size

2.4. Components of a Fuel Cell

In order for FC to produce electricity; an ionic conductive membrane, catalyst layer for anode and cathode reactions, porous gas diffusion layer that can allow homogeneous distribution of gases at the anode and cathode, and electro porous bipolar plate with electrical conductivity, including flow channels through which gases are fed at the anode and cathode. and a current collector plate are required to collect current. There are certain features that these elements must provide. The anode, cathode, and electrolyte combined from these parts are given a special name and are called membrane electrode assemblies (MEA). However, some resources include the gas diffusion layer (GDL) in the MEA. In order to avoid misunderstandings, many researchers state the number of layers and say MEA with 3 or 5 layers. Throughout this study, when MEA is mentioned a 3-layer structure, namely anode, cathode and membrane, will be meant. For a descriptive visual, please refer to Figure 7 below.

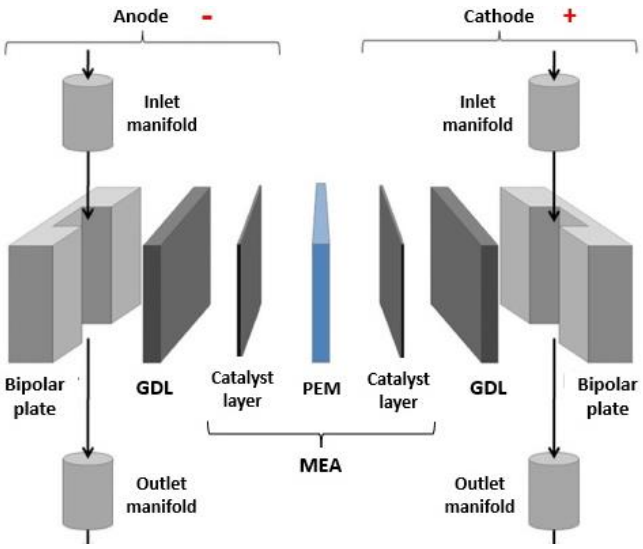

Figure 7: Parts of a PEMFC

2.4.1. Membrane

In case of PEMFC, it is necessary to use a membrane that has high ionic conductivity, does not allow gas passage, does not conduct electricity, can withstand a certain mechanical load, its thermal expansion is below a certain value. The most common commercial product that can respond to these requests appears to be Nafion. It is obtained by adding hydrophilic sulfonic side bonds to Teflon (PTFE), a hydrophobic fluorinated polymer. [12]

H^+ ion formed in the anode side in PEMFC passes through the Nafion membrane and reaches the cathode side. There are two types of mechanisms inside the Nafion that allow the movement of the H^+ ion. These are the transport and transmission (Grotthuss) mechanisms. In the transport mechanism, the H^+ ion sticks to the water and forms the H_3O^+ ion and moves to the cathode side by the anode through diffusion from the puddles in the structure of Nafion. Nafion needs to be moistened well for the transport mechanism to work. In the transmission mechanism, it acts by bonding with H^+ ion acts by bonding with minus charged sulfonic groups (SO_3^-) and passing from one end to the other. In order to achieve the highest performance in FCs, moist gas should generally be used. [12]

2.4.2. Catalyst Layers

Reaction taking place in the anode and cathode parts of the PEMFC have been mentioned before. On anode side, in which hydrogen gas decomposes into ions and electrons, takes place very easily with a good catalyst since the activation energy is very low and high equilibrium current density can be achieved. The cathode reaction is a more difficult than the anode

reaction. For this, more effective catalysts should be used on the cathode side. It is desired that the reactions on the anode and cathode sides are at the same speed. In this case, either a lower activity catalyst is used on the anode side, generally being cheaper, or the amount of catalyst charge on the anode is kept low. Thus, the cathode reaction is prevented from being a limiting step. [12]

Anode and cathode catalyst layers consist of catalyst, Nafion ionomer and voids, together with the backing materials. In these layers, reactions take place on the surface of the catalysts. In order for the reaction to take place in both layers, ions, electrons and gases must reach or be removed from the catalyst surface. While H_2 gas reaches the catalyst surface on the anode side, the H^+ ion released as a result of the reaction moves from the Nafion ionomer that is randomly distributed in this layer to the Nafion membrane, and the electron released after this reaction reaches the gas diffusion layer over the carbon support material. On the cathode side, O2 gas reach the catalyst surface from the cavities, H+ ion from randomly distributed Nafion ionomers in the catalyst layer, and electrons from the gas diffusion layer reach the catalyst surface via carbon support. The water formed in this region is thrown out of this layer from the cavities. These regions, where the reactions take place, and where gas, ion and electron access can be provided, are called triple points. The reaction does not take place unless full ion, electron or gas access cannot be achieved, and in that case, this zone lowers the average voltage of that electrode. [12] The structure of the catalyst layer is schematically shown in Figure 8 below. In order to obtain the highest efficiency from the catalyst layer, it should be both porous and the ionomers and catalysts should be in a homogeneously distributed structure.

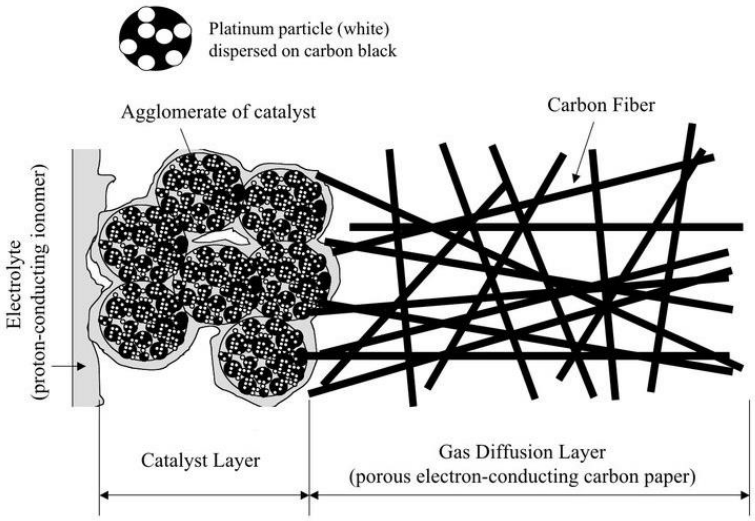

Figure 8: Catalyst layer and GDL structure

2.4.3. Gas Diffusion Layer (GDL)

The GDL is in between catalyst layer and bipolar plates and Figure 8 can be referred for its structural scheme as well. There are some features expected from GDL in FCs and these are:

- Distributing the gas coming with the bipolar plate homogeneously to the anode and cathode layers.
- Ensuring that the electrons used or produced in the anode or cathode reach the required places.
- To ensure that the heat generated in the anode or cathode is removed from these layers.
- To reduce the contact resistance between the catalyst layer and the bipolar layer.
- Preventing the membrane from tearing by the bipolar layer during compression or stretching of the membrane into the gas flow channels.

It has a porous, conductive and hydrophobic structure as it should be in a structure that can allow gas, electron, water and heat transfer. There are materials called carbon paper and carbon fabric with these properties. Both materials are made of carbon fibers, in one, carbon fibers are pressed and the other is woven like a fabric. [13]

In order to reduce the contact resistance in GDL and to ensure that the water formed on the surface is removed quickly, surface to be in contact with the catalyst is covered with carbon in a way that the surface is microporous.

2.4.4. Bipolar Plates

In cases where it is desired to connect multiple FCs in series, different gases are fed to the anode of one cell and to the cathode of the other cell on the same plate. By doing so, the electron produced in the anode layer during the transfer of electrons can move to the cathode of the next cell in the fastest way and with the least loss without passing through any extra layers. These plates have the same charge as the anode of one cell, while they are the same as the cathode of the other cell. Meaning that, the side facing one cell is a negative charge, while the side facing the other cell is a positive charge for that cell. For this reason, these plates are called bipolar plates [12]. There are certain features that bipolar plates should have, and their reasonings are as follows:

- High electrical conductivity for electron transfer between cells

- Low gas permeability in order to avoid loss of both fuel and voltage in case two different gases pass to each other side
- Mechanical durability to provide structural durability
- Light weight for portable applications
- High thermal conductivity for removing heat generated in the FC
- Malleability to process flow channels used to feed gases fed into FC
- Resistance to corrosion to withstand the acidic, hydrogen and oxygen gases in the fuel cells and where different stresses are formed

Certain materials with these properties, stress and corrosion resistance, stand out. A lot of research is being done on graphite polymer composite plates and metallic plates that provide all these features. Corrosion and contact resistance values can be improved by making different coatings on the surface of metal plates. [12]

2.4.5. Gasket

In case of PEMFC, a gasket material that can prevent gases from leaking out of the desired areas, can withstand acidic environments and high compression pressure should be used. Moreover, it should not react with hydrogen and oxygen and be resistant to melting and breaking. Finally, the gasket must not contain materials that can poison the catalysts. Silicone and Teflon gaskets can provide these properties to a great extent.

2.4.6. Current Collecting Plates

PEMFCs are so called electronic accumulating plates, which are placed at the beginning and end of the FC stacks. These plates are the (-) and (+) poles of the FC stacks. Highly conductive materials such as gold-plated copper plates are used for this purpose.

2.5.Fuel Cell Module

Throughout the project, FC module from DEVINN s.r.o., with maximum net power output of 30 kW, has been used. The module consists of FC stacks, coolant pump, coolant tank, particulate filter, drain valve, sensors for temperature, hydrogen voltage and current, DC/DC converter, control unit and safety devices as basically shown in Figure 9. [14]

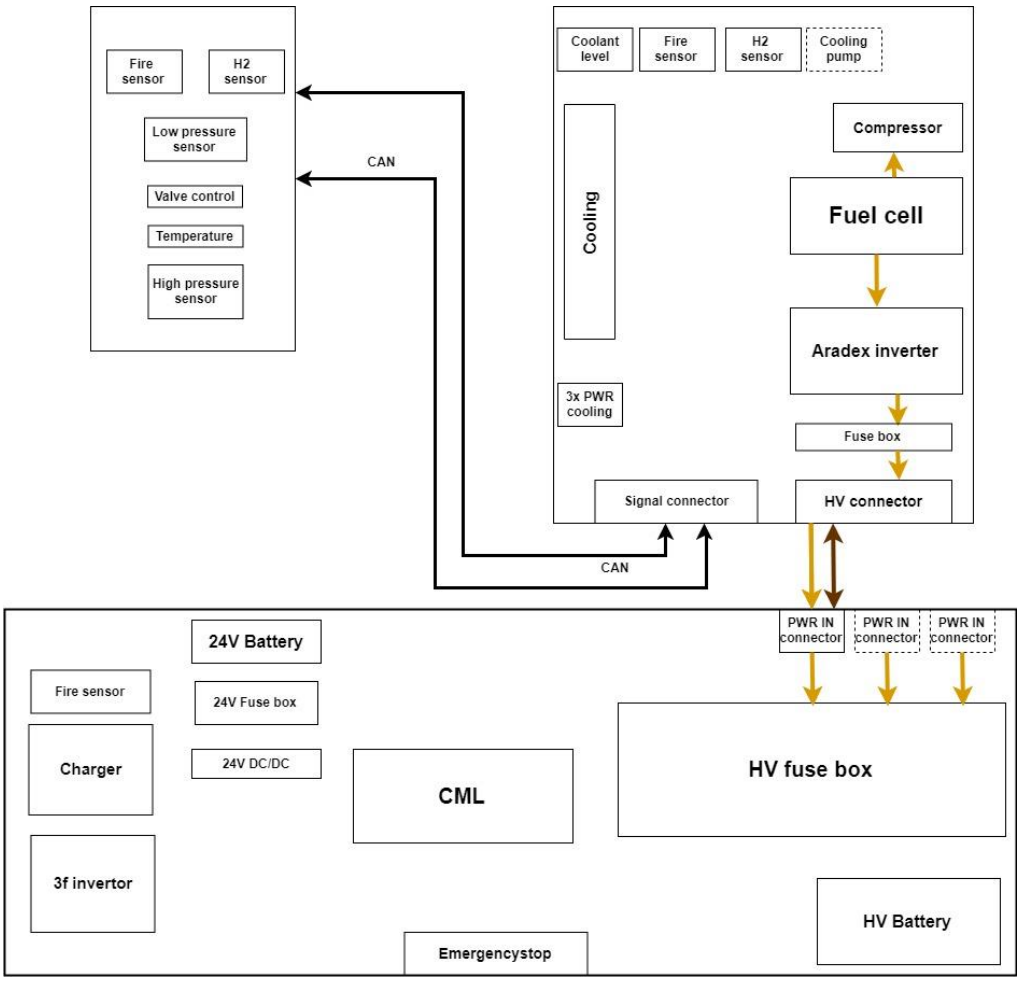

Figure 9: DEVINN s.r.o. Fuel Cell module scheme

The module further consists of high voltage battery, 24V battery, fuse box for both batteries and a central control unit (CML). Sensors for monitoring p, T, H_2 and to make sure safety of the system are connected to module via signal connectors. [14]

2.5.1. Compressor

Air compressor delivers air flow, which is measured by the mass flow sensor, to the FC stacks. Despite the fact that compressors for conventional systems and FC applications have numerous common features; in case of an automotive application, standard compressor can't be utilized on a FC powered vehicle due to additional compressor requirements such as higher efficiency, lower flow rate and so on. To select the ideal air compressor for a chosen FC system, different types of compressors are investigated. They are screw compressors, scroll compressors, roots compressors and turbo compressors. [15]

Based on theoretical and experimental results, turbo and roots compressors have better performance than the other types. However, due to restricted pressure ratio, roots compressors are less common than turbo compressors in FC vehicle applications. [15]

2.5.2. Pump

One of the major parts of a FC system is pump. It is also essential for the cooling system. The reason is that a pump is needed to deliver the fuel and the coolant to the system. However, it requires a power to do so and this power loss affect the FC efficiency. Hence, depending on the system application, an appropriate pump has to be selected to keep power loss low and system efficiency moderately high. [16]

2.5.3. Ion Exchange Filter

Ion exchange filter forms deionized water by expelling ions from FC water even under extreme ecological conditions. It is needed to maintain low conductivity and offers minimized pressure drop and optimum resin consumption to obtain prolonged lifetime. [17]

2.5.4. Battery

The system needs to draw current and be supplied voltage by the batteries to sustain operation of the electrical accessories as well as to power the additional module components such as the compressor and pump. As shown above in Figure 9, 24V and high voltage (HV) batteries are integrated to the FC via connectors and inverters.

The specific battery being used in DEVINN hydrogen FC module is shown in Figure 10 and its parameters are given in Table 2. [14]

Table 2: DEVINN FC module battery properties

Max. Power	100	kW
Nominal Voltage	60	V
Capacity	8.5	kWh
Cooling	Air cooled	
Features	BMS with CAN communication, isolation monitoring, current measurement	

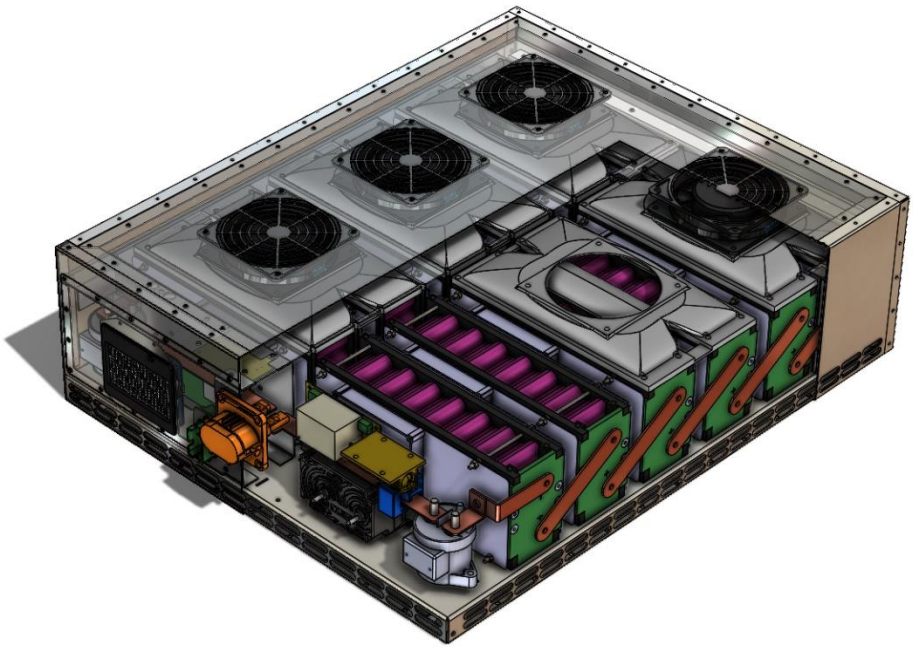

Figure 10: DEVINN battery pack

2.5.5. DC/DC Inverter

FC system requires a DC/DC inverter device to condition the power and to emulate the system by reproducing output current and voltage characteristics. There are several types of DC/DC inverters which are fly back converter, push pull converter, half bridge converter and full bridge converter. Among these, full bridge type is preferred due to its capability to allow higher power input and having lower ohmic resistance. [18]

2.5.6. Control Unit

Central control unit (labeled as CML in Figure 9) in FC systems are essential to monitor system operation and safety. CML has its own subsystems to manage thermal operation, air and water supply systems and to control H_2 supply in order to achieve optimum power rates under safe mechanical and electrical operating conditions.

3. Cooling and Heat Accumulation of the FC system

At the end of FC reaction, heat is also produced as byproduct and this heat generated must be removed in order to sustain temperature homogeneity within cells as mentioned in previous sections. Cooling system's importance comes from the temperature uniformity within stack which is essential in a way that it directly affects performance characteristics of the FC [14].

Throughout this study, simplified coolant system shown below in Figure 11 is considered for the selected FC module.

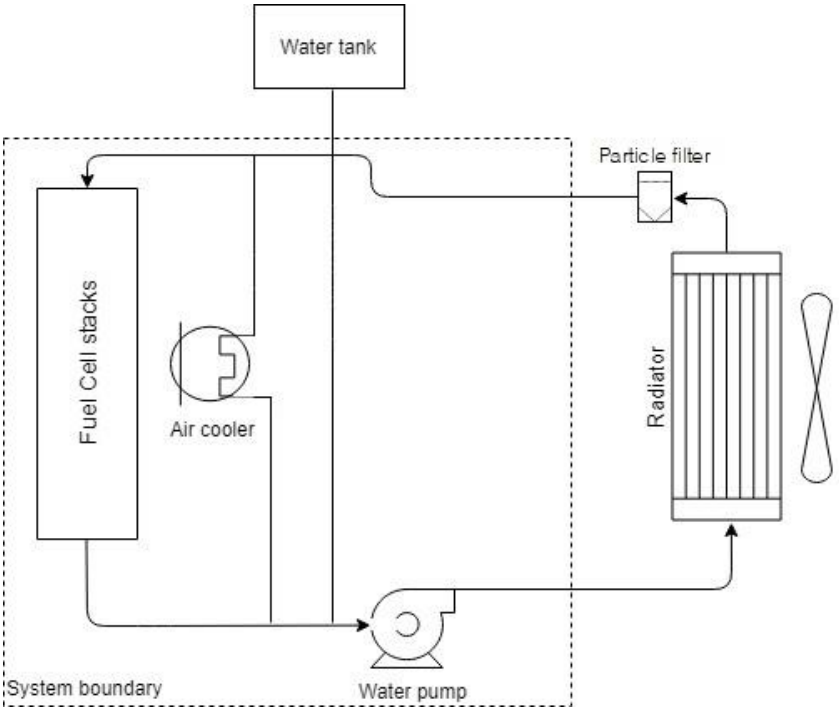

Figure 11: FC module coolant system

3.1. Cooling Strategies

There are several solutions for cooling of FC. In case of PEMFC, significant part of the heat generated is rejected with a cooling method. These cooling methods depend on the stack properties and purpose of usage.

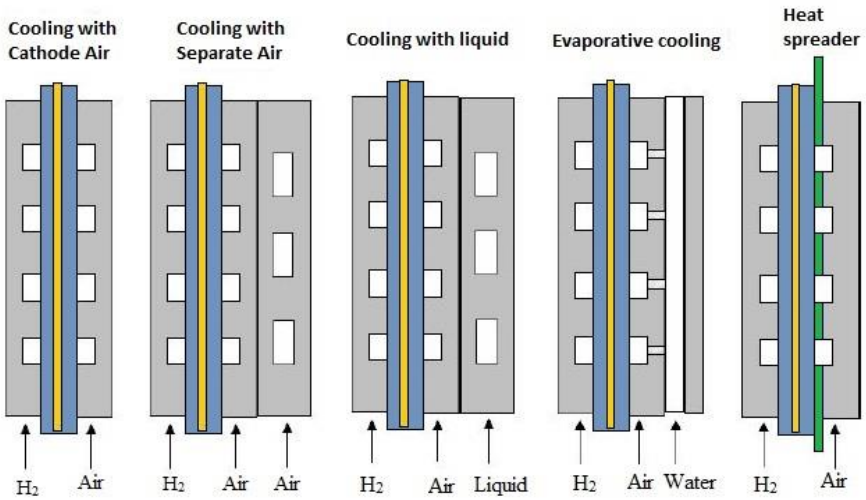

Figure 12: Cooling strategies

Moreover, cooling strategies depend on several more factors being system design, are of usage and how much heat is needed to be rejected. For instance, air can cool down smaller systems with low power outputs because such systems have simple design without a cooling circuit and heat exchanger. On the other hand, cooling with liquid is required for FC systems with greater power output since the cooling system has more components and less limits. It is also because that liquid as a cooler has a higher thermal conductivity and capacity, meaning that heat rejection rate is higher. Each of them is in accordance with the FC power output and has benefits and drawbacks are tabulated below in Table 2 and shown above in Figure 12. [19]

Table 3: Possible solutions for cooling of PEMFC [19]

FC P_{out}	Cooling method	Benefits	Drawbacks
<200 W	Cooling with cathode air	Simpler system design Economical Does not require a coolant loop	Heat cannot be removed via free convection Larger weight and area occupied
200 W - 2 kW	Cooling with air (separate from cathode air flow)	Simpler system design Low standby power Does not require a coolant loop	Not a practical approach to FC cooling Standby power limits cooling performance
≈1000 W	Cooling with heat spreaders	Low standby power Increased system reliability	Thermal length is limited Very good thermal conductivity needed
	Cooling with phase change	Does not require a coolant pump Reduced flow rate of the coolant	Flow instability
	Cooling through boiling	Uniform working temperature	Requires specific coolant
500 W - 100 kW	Evaporative cooling	Simpler system design Cold start	Complex design Control of water evaporation rate
>10 kW	Liquid cooling	Higher cooling capacity Good cooling rate control Suitable to automotive industry applications	High standby power Extra tools may be required Radiator size

FC power output is the major factor in choosing suitable cooling strategy. Cathode air cools down the stack if the power generated is less than 200 W whereas separated air flow is needed for the stacks producing power from 200 to 2000 W.

As mentioned, liquids have higher specific heat capacity, conductivity and generally heat transfer coefficient than gases. Hence, they are preferred as coolant for higher load applications such as PEMFC stacks producing 10 kW or more of power. The mostly frequently used cooling strategies with liquid as coolant consist of convection to dissipate heat in cooling plates or channel which could be designed with fins to increase heat transfer rate. Heat transfer occurs through bipolar plate to the liquid that streams within cooling plates or channels. Liquid is then heated up and sent to heat exchanger via pump so that the waste heat can be rejected or used in different purposes. As shown in Figure 13Table 3, due to required extra components such as water pump and drain valve, liquid cooling is more costly and heavy. [19]

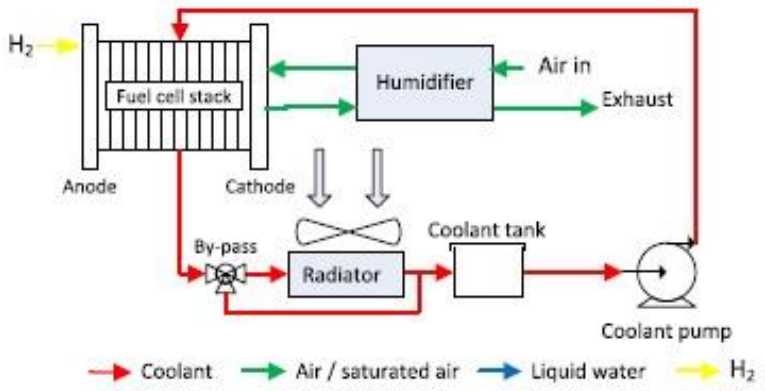

Figure 13: System layout of cooling with liquid [20]

In cooling with phase change applications use the enthalpy of vaporization to reject the heat from FC. It can be achieved through boiling and evaporative cooling. Enthalpy of vaporization is achieved with additional water that is added to flow channels of PEMFC to cool the electrodes and to use this heat for the phase change. This strategy prevents FC membrane from drying and it eliminates usage of humidifier and another cooling plate. However, it requires a condenser to recover the evaporated water as seen in Figure 14. [20]

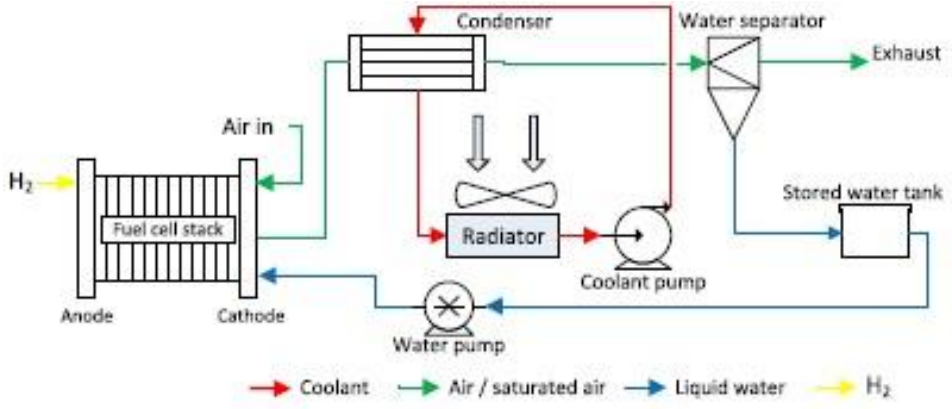

Figure 14: System layout of evaporative cooling

3.2.Heat Management of Fuel Cells

One of the products of PEMFCs is heat. The heat generation results from condensation of the water vapor, reversible heat from the electrochemical reactions, reaction irreversibility and electrical resistance. 2nd law of Thermodynamics explains the reversible heat as the difference between chemical energy of the reactants and useful energy. [19]

PEMFCs operate at relatively lower temperatures and in case higher operating temperature is reached, product water will vaporize more. Hence, there will be less amount of liquid water due to increasing latent heat of vaporization. To maintain homogeneous temperature, radiator rejects the waste heat and to do so, cooling systems explained in section 3.1 are used. FCs can also be cooled without using energy via fins and passive heat exchangers. [2]

3.2.1. Fuel Cell Energy Balance

To express the energy balance of the FC, reactants and products should be categorized with their phases as shown in Figure 15. Afterwards, specific enthalpy of the reaction variables needs to be governed as well as their flow rates for which mass balance equations may be needed to use. Specific enthalpy can be calculated as a function of p,T,M and $\dot{m}$. Accordingly, the energy balance equiation is written and solved. [21]

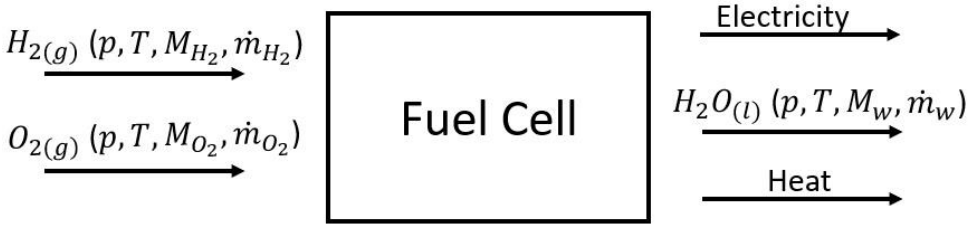

Figure 15: FC energy balance scheme

Chemical reaction of H_2 and O_2 that results in water generation is given as

$$H_2 + {}^1\!/_2\, O_2 \rightarrow H_2O \qquad \text{Eq.1}$$

According to the Stodola, general energy balance of the FCs is electric power and input and output sums of enthalpy. This energy balance is as follows [22]

$$\sum (H_i)_{in} = W_{el} + Q_{dis} + Q_{cool} + \sum (H_i)_{out} \qquad \text{Eq.2}$$

Once chemical reaction energy is equated to the energy of electricity produced and the heat [2]

$${}^1\!/_{2F}\, H_{HHV} n_{cell} = Q_{gen} + I_{cell} V_{cell} n_{cell} \qquad \text{Eq.3}$$

Dry gas enthalpies are calculated from

$$H = \dot{m} c_p \left(T - T_{ref}\right) \qquad \text{Eq.4}$$

In case the gas has a higher heating value (HHV), enthalpy is calculated as

$$H = \dot{m} c_p \left(T - T_{ref}\right) + H^0_{HHV} \qquad \text{Eq.5}$$

where H^0_{HHV} is the HHV of the gas at 0°C. However, we might have to calculate HHVs unless they are required at room temperature which is assumed as 25°C [21]. Then, water vapor enthalpy is

$$H = \dot{m}_{w(g)} c_{p,w(g)} \left(T - T_{ref}\right) + H^0_{fg} \qquad \text{Eq.6}$$

and the liquid water enthalpy

$$H = \dot{m}_{w(l)} c_{p,w(l)} \left(T - T_{ref}\right) \qquad \text{Eq.7}$$

3.3.Heat Exchangers for Fuel Cells

Heat exchangers (HEs) are needed for FC stacks operating at low temperatures (i.e. PEMFCs) to reject the heat from renewed reactant which is vital for the system efficiency. Thermal stresses under varying load and operating conditions should be acknowledged as a design

criterion. The number of HEs required for cooling depends on amount of power generated by the FC stack.

In case of liquid cooling where the power production is higher, heat transfer from the cathode air can be neglected. Hence, all the heat has to be rejected by the radiator. However, when compared to conventional automotive radiators, radiators of the liquid cooling systems of FC stacks are larger in size. This is because temperature difference between the heated liquid and the air in cathode is much less than in automotive applications. PEMFCs require cooler to manage the inlet air. HEs for this purpose are (See Figure 13): [23]

- Humidifier for cathode inlet
- Condenser for cathode outlet

For the fuel processing in PEMFCs, HEs are used to cool down the H_2 and to recover the exhaust gas heat. [23]

3.3.1. Heat Exchanger Modelling

Heat transfer to the cooling liquid is derived as

$$\frac{dQ_{cool}}{dA_{cool}} = U(T_s - T_{cool}) \qquad \text{Eq.8}$$

Similar correlation applies for HEs. However, in this case, the heat transfer coefficient is not local but overall

$$Q_{cool} = UA(CF)LMTD \qquad \text{Eq.9}$$

Where CF is the correction factor and LMTD stands for logarithmic temperature difference and as defined as [2]

$$LMTD = \frac{(T_w - T_a)_i - (T_w - T_a)_o}{ln\frac{(T_w - T_a)_i}{(T_w - T_a)_o}} \qquad \text{Eq.10}$$

In case the difference between T_s and T_{cool} is not constant, heat transfer to the cooling liquid is described as

$$\dot{Q}_{cool} = \dot{m}_a c_{p_a}\left(T_{a_o} - T_{a_i}\right) = \dot{m}_w c_{p_w}(T_{w_i} - T_{w_o}) \qquad \text{Eq.11}$$

Difference in T_{cool} above depends on how much heat is produced and amount of water vaporization. To sustain temperature homogeneity within the stack, the difference should be minimized. [21]

The required HE results can be obtained by transformation of different unknowns and variables than of LMTD approach. This approach is called ε-NTU method. It is the same method as LMTD, yet the variables being transformed are different [24]. It's relation to heat transfer rate is

$$\dot{Q} = \varepsilon C_{min}(T_{w_{in}} - T_{a_{in}}) \qquad \text{Eq.12}$$

where ε is the effectiveness that depends on heat capacity, NTU and flow type. It is defined by the ratio of the heat rejected to the possible heat transfer. Heat capacity ratio [24]

$$\varepsilon = {}^{Q}/_{Q_{max}}$$
$$C_i = \dot{m}_i c_{p_i} \qquad \text{Eq.13}$$

Through this project, both LMTD and ε-NTU methods will be performed.

4. Methodology and Results

In this section of the report, the obtained results, methodology behind the designs and sensitivity analysis will be discussed.

Before starting the calculations and engineering design of the cooling system parts, the initial boundary conditions or the design limitations had to be derived. The parameters that the designs are based on are given below in Table 4 [14],

Table 4: Initial conditions

Given	Value	Unit
$\dot{Q}_{gen_{min}}$	7.5	kW
$\dot{Q}_{gen_{max}}$	44.5	kW
$T_{w_{in}} = T_{rad_{in}}$	73	$°C$
$T_{w_{out}} = T_{rad_{out}}$	60	$°C$
$T_{a_{in}}\ (Confidential)$	x:y	$°C$
$T_{a_{out}}\ (Confidential)$	x:y	$°C$
$Best\ case\ dimensions$	196 x 650 x 850	mm

$Worst\ case\ dimensions$	200 x 800 x 1200	mm
$\dot{V}_w\ (Confidential)$	x:y	lpm
$Required\ \dot{Q}_{rad_{avg}}$	36.44	kW

Throughout this project, the design calculations were held in accordance with the mean parameters being, mean flow rate, mean temperature range and mean heat rejection. It should be noted that, heat rejection parameters given above are net power output of the FC module. In order to calculate the mean required heat rejection, which is the base parameter that the radiators should be designed accordingly, the relation given in Eq.3-12 was used.

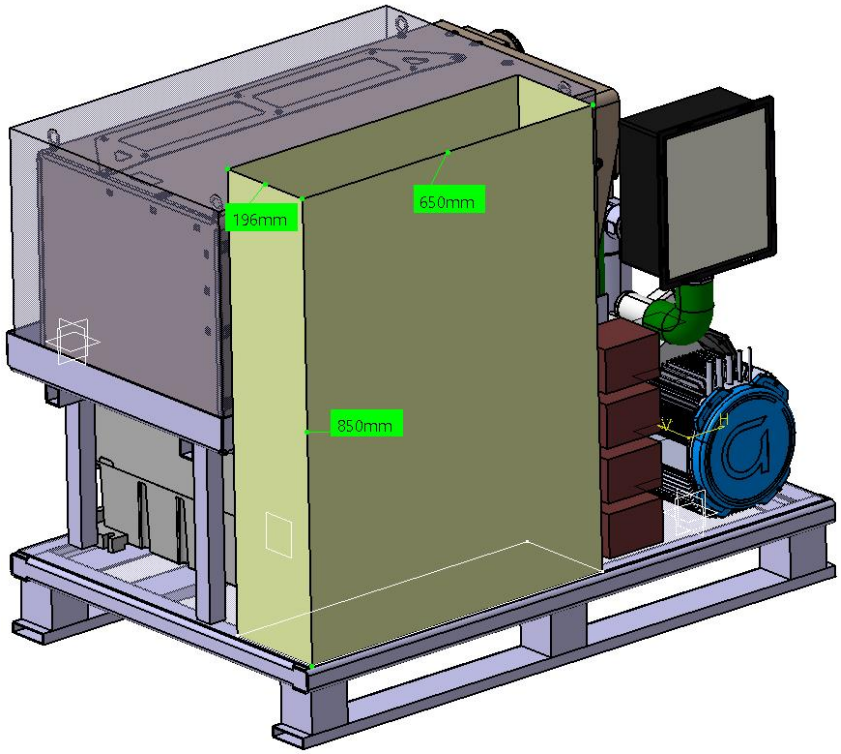

Figure 16: Space requirement for the radiator

Figure 16 above shows the space that is planned for the radiator to be placed in the best case. This space requirement is taken into consideration when choosing the geometrical parameters of the radiators designed.

As mentioned in the previous section of the report, both LMTD and ε-NTU methods are applicable in heat exchanger designs. LMTD method can be applied when the purpose is to size the heat exchanger, radiator in our case, and when the inlet and outlet temperatures as well as the flow rates are known. On the other hand, ε-NTU method can be applied when the aim is to obtain outlet temperatures as well. In this project, inlet and outlet temperatures and flow

rates are known as initial conditions of the radiator design. Hence, both methods will be applied in this project to show the applications with variety purposes.

4.1.Design Nº 1

The first design is a universal aluminum radiator with flat tubes and rectangular fins. The flow arrangement is selected as crossflow where the flow of air and the coolant, water, are perpendicular to each other. The air is inducted into the radiator via fans and the coolant, deionized water, is pumped through the tubes and the heat is rejected from the water by the cold fluid, air. As a result of this process, convection from the internal flow of water within tubes and convection from external air flow occur.

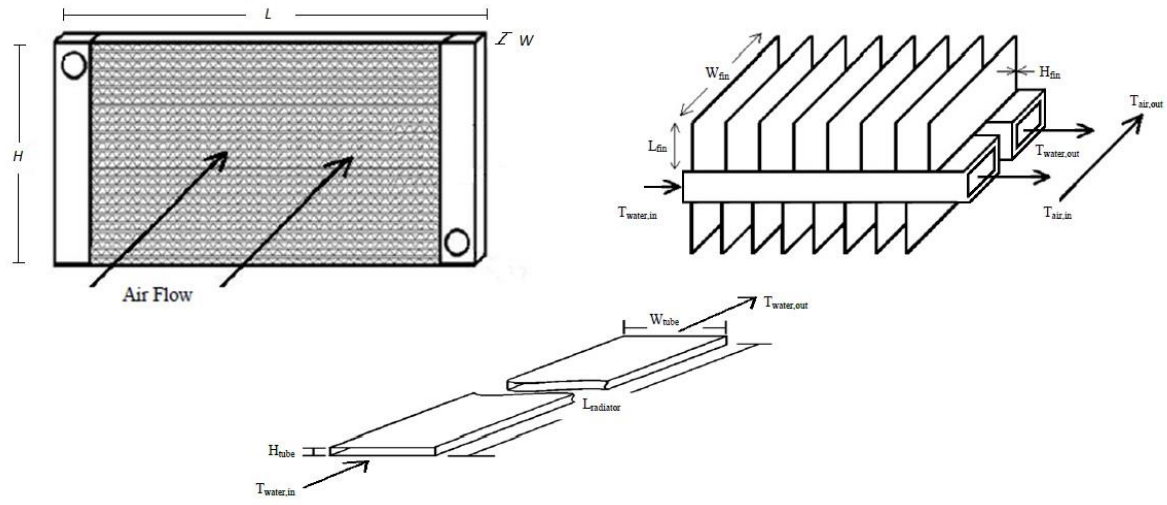

Figure 17: Schematic of radiator #1

Figure 17 shows the schematic of the assumed radiator geometry including the assumed fin and tube geometries. The design is based on ε-NTU method and the steps taken to achieve the result will be explained in the upcoming parts of this section of the report. Below in the Table 5, input parameters of the calculations are given. Heat exchanger fouling factor due to using water as a cooling liquid was assumed and shown below as well.

Table 5: Input parameters for design #1

Inputs	Value	Unit
W_r	100	mm
L_r	650	mm
H_r	800	mm
W_t	30	mm

H_t	3.75	mm
L_t	650	mm
W_f	70	mm
h_f	0.55	mm
L_f	5	mm
N_t	140	[-]
N_f	750	[-]
k_{al}	205	$W/_{mK}$
R_f	0.0002	$W/_{mK}$

Having known the inlet and outlet temperatures of the both fluids, thermal properties of them can be obtained at the average air and water temperatures which will later be used to define internal water and external air flow correlations. Table 6 and Table 7 show these thermal properties of water and air, respectively.

Table 6: Water thermal properties from Incropera

Water Properties at average T_w		
ρ_w	979.63	$kg/_{m^3}$
c_{p_w}	4188	$J/_{kgK}$
k_w	0.658	$W/_{mK}$
μ_w	$4.22x10^{-4}$	$Pa/_s$
Pr_w	2.681	[-]

Table 7: Air thermal properties from Incropera

Air properties at average T_a		
ρ_a	1.101	$kg/_{m^3}$
c_{p_a}	1007.7	$J/_{kgK}$
k_a	$2.76x10^{-2}$	$W/_{mK}$
μ_a	$1.93x10^{-5}$	$Pa/_s$
ν_a	$1.77x10^{-5}$	$m^2/_s$
Pr_a	0.705	[-]

Values in the tables are taken from thermophysical property tables of matters [25]. The Prandtl number can either be taken from aforementioned tables or be calculated as a function of dynamic viscosity, specific heat capacity and thermal conductivity by using Eq.15 below.

$$Pr_{a,w} = \frac{\mu_{a,w} c_{p_{a,w}}}{k_{a,w}} \qquad \text{Eq.14}$$

In order to derive heat transfer coefficients, internal water flow and external air flow correlations have to be derived. The geometric properties of the areas where air and water are in contact with are essential to do so. The tube cross-sectional area and its perimeter are given in Eq.16

$$A_t = W_t H_t$$
$$P_t = 2W_t + 2H_t \quad \text{Eq.15}$$

The surface area of the radiator is calculated in a similar way to the tube's cross-sectional area

$$A_r = L_r H_r \quad \text{Eq.16}$$

Adiabatic fin tip can be used to obtain more accurate heat transfer results and to do so, corrected fin length for rectangular fin geometry is defined [25]

$$L_c = L_f + {}^{H_f}/_{2} \quad \text{Eq.17}$$

Other geometric terms being single fin surface area, base surface area and total fin&base surface area of a single tube are given below in Eq.19

$$A_f = 2W_f\, L_c$$
$$A_b = 2L_{rad}W_t - H_f W_f N_f \quad \text{Eq.18}$$
$$A_{fb} = N_f A_f + A_b$$

Moreover, total external and internal areas have to be calculated to derive overall heat transfer coefficient multiplied by area. These external and internal areas are defined as

$$A_{ext} = A_{fb} N_t$$
$$A_{int} = (2W_t + 2H_t) L_t N_t \quad \text{Eq.19}$$

The results obtained from the calculations by using Eq.16-20 are listed in Table 8.

Table 8: Area calculation results

Parameter	Value	Unit
A_t	$1.125x10^{-4}$	m^2
P_t	0.067	m
A_r	0.52	m^2
L_c	0.005	m
A_f	$7.03x10^{-4}$	m^2
A_b	0.019	m^2
A_{fb}	0.57	m^2
A_{ext}	79	m^2
A_{int}	7.6	m^2

From the known values of volumetric flow rate and calculated mean required heat rejection, mass flow rates can be derived by using simple relation given as

$$\dot{m} = \dot{V}\rho \qquad \text{Eq.20}$$

The next step before calculating the internal water flow and external air flow correlations is to obtain total thermal capacities of both fluids and total thermal capacity ratio. To do so, relations given in Eq.22 are used [25]

$$\begin{aligned} C_{a,w} &= \dot{m}_{a,w} c_{p_{a,w}} \\ C_r &= \frac{C_{min}}{C_{max}} = \frac{\min(C_a, C_w)}{\max(C_a, C_w)} \end{aligned} \qquad \text{Eq.21}$$

Convective heat transfer occurs due to internal water flow and external air flow. To start with the internal water flow, we can define it as the flow of hot water travelling in the bounding passages of rectangular tubes with constant cross-sectional area [24]. Since non-circular tube geometry is used in this design, a hydraulic diameter needs to be defined, which will later on be used to estimate the Reynolds number.

$$D_h = {}^{4A_t}/_{P_t} \qquad \text{Eq.22}$$

Reynolds number defines the flow properties; however, it is function of not only hydraulic diameter but also flow velocity, density and dynamic viscosity (See Table 6). Hence, the velocity of water within the tubes has to be calculated and Reynolds number is calculated by the following relations

$$\begin{aligned} u_w &= \frac{\dot{V}_w}{N_t\, A_t} \\ Re_w &= \frac{\rho_w u_w D_h}{\mu_w} \end{aligned} \qquad \text{Eq.23}$$

The Reynolds number was obtained as approximately 671 which is less than the critical Reynolds number, $Re_{cr_{int}} \approx 2300$, meaning that the internal flow is fully developed laminar flow. For such a flow, and for a rectangular tube with constant cross-sectional area, Nusselt number is 5.6 [26]. Having obtained all the needed parameters, convective heat transfer coefficient (HTC) of water can be calculated as

$$h_w = \frac{Nu_w k_w}{D_h} \quad \text{Eq.24}$$

As aforementioned, another source of convection is the external air flow. This flow can be defined as an unbounded flow of cold air over the solid surfaces [24]. Since the aim is to calculate the HTC of air, similar parameters to the water flow need to be derived. Regarding the air velocity, the total area that the air is contact with is different than of the water. Hence, the relation to define velocity of air through each tube differs and given in Eq.26 below

$$u_a = \frac{\dot{V}_a}{A_r - (N_t H_t H_r)} \quad \text{Eq.25}$$

In case of internal water flow, the characteristic length to define the Reynolds number is the hydraulic diameter. However, in external air flow, flow length corresponds to the width of the fins (See Figure 17). To obtain Reynolds number of air, relation below yields

$$Re_a = \frac{u_a W_f}{\nu_a} \quad \text{Eq.26}$$

The calculated Reynolds number is $6.48x10^4$ and less than critical Reynold number, $Re_{cr_{ext}} \approx 5x10^5$, shows that the air flow is laminar. Thus, the relation to express Nusselt number is [27]

$$Nu_a = 0.664\, Re_a^{0.5}\, Pr_a^{0.33} \quad \text{Eq.27}$$

After deriving the required parameters, HTC of air can be calculated by using

$$h_a = \frac{Nu_a k_a}{W_t} \quad \text{Eq.28}$$

Table 9: Obtained results

Parameter	Value	Unit
$\boldsymbol{D_h}$	0.007	m
$\boldsymbol{Re_a}$	$6.48x10^4$	$[-]$
$\boldsymbol{Re_w}$	671	$[-]$
$\boldsymbol{Nu_a}$	150.5	$[-]$
$\boldsymbol{Nu_w}$	5.6	$[-]$
$\boldsymbol{h_a}$	138.67	W/m^2K
$\boldsymbol{h_w}$	554.16	W/m^2K

From the obtained results, one can see that the Reynolds number of air is greater than of the water since air is flowing much faster over the surfaces it is in contact with. Hence, resulting Nusselt number yields a greater value for air as well. Another conclusion to be made is that the HTC of water is higher than of the air as expected. It means that more heat is rejected by the coolant than the air. The reason behind this is, thermal conductivity and specific heat capacity of water is greater than the ones for air (See Table 6 and Table 7).

Another essential evaluation parameter for the air side heat transfer is the increased heat transfer area by using fins. Even if it is an advantage, fins are conductive resistance sources and, hence, their efficiency has to be taken into account to see if the heat transfer is enhanced with the selected fins in terms of their type and geometry. [25]

In order to evaluate the fin efficiency, correlations from thermodynamics and/or heat transfer can be used. Fin efficiency is function of corrected fin length and fin effectiveness coefficient, m. Having known that fins used in this design are assumed as straight and rectangular, following equations can be derived [24]

$$\eta_f = \frac{\tanh(mL_c)}{mL_c}$$
$$m = \sqrt{\frac{2h_a}{k_{al}H_f}} \qquad \text{Eq.29}$$

Once the fin efficiency is obtained, overall surface efficiency, η_o, is calculated which will later be used to find overall heat transfer coefficient. It is also used to take the imperfections caused by the external air flow about the finned areas into account. Eq.31 yields the following to define η_o

$$\eta_o = 1 - \left(N_f \frac{A_f}{A_{fb}}\right)\left(1 - \eta_f\right) \qquad \text{Eq.30}$$

Before obtaining the final results regarding the heat rejection rate of the radiator and the outlet temperatures, correlations of the selected ε-NTU method have to be applied. First, the overall HTC multiplied by the heat transfer area, total conductance, is calculated as

$$UA = \frac{1}{\frac{1}{\eta_o U_a A_{ext}} + \frac{1}{U_w A_{int}} + R_f} \qquad \text{Eq.31}$$

Afterwards, NTU is derived as a function of UA and the minimum thermal capacity, so that the effectiveness, ε, can be obtained. To do so, Eq. 33 is applied, and it yields

$$NTU = \frac{UA}{C_{min}}$$
$$\varepsilon = 1 - exp\left(\left(\left(\frac{1}{Cr}\right) * (NTU^{0.22})\right) * (exp(-Cr * NTU^{0.78}) - 1)\right) \quad \text{Eq.32}$$

Having obtained required parameters, heat rejection by the radiator can now be calculated by using the equation below

$$\dot{Q}_{ideal} = C_{min}(T_{w_i} - T_{a_i})$$
$$\boldsymbol{\dot{Q}_{rad}} = \varepsilon \dot{Q}_{max} \quad \text{Eq.33}$$

whilst the outlet temperature of both air and water is then derived from

$$T_{w_o} = T_{w_i} - \frac{Q_{rad}}{C_w}$$
$$T_{a_o} = T_{a_i} + \frac{Q_{rad}}{C_a} \quad \text{Eq.34}$$

Table 10: Major results

Parameter	Value	Unit
$\boldsymbol{\eta_f}$	0.972	[−]
$\boldsymbol{\eta_o}$	0.978	[−]
$\boldsymbol{UA}$	≈ 1890	$W/_K$
NTU	1.04	[−]
$\boldsymbol{\varepsilon}$	0.53	[−]
$\boldsymbol{T_{a_o}}$	55.13	℃
$\boldsymbol{T_{w_o}}$	59.91	℃
$\boldsymbol{\dot{Q}_{rad}}$	36.7	kW

The reason why the ideal, so called maximum possible, heat transfer is calculated is that we need it to derive the heat transfer by the radiator by relating it with the effectiveness. The typical automotive radiator has the temperature effectiveness between 35-40% and the results of this design yield that the designed radiator has a greater effectiveness, 53%, when compared to its equivalents in the market. [27]

The input outlet temperature values for the design were not exactly as same as the obtained outlet temperature results. However, the difference is much less than order of magnitude, in Celsius degrees. Hence, it is neglected due to lack of importance and resulted in an acceptable outlet temperature. Most importantly, the required heat rejection under mean operating conditions is satisfied with the designed radiator. As it is seen in Table 4, required heat rejection rate is 36.44 kW and the design radiator is able to reject 36.7 kW.

Apart from the methodology that has been explained so far, another design parameter has an important role on the overall process as well. That is the pressure drop for both air and water sides. To do so, friction factor and the mass flux parameter G which is based on minimum free flow area need to be estimated. [26] For the water side, it yields

$$G_{a,w} = \rho_{a,w} u_{a,w}$$
$$f_w = (0.79 \log(Re_w)^{-1.64})^{-2} \quad \text{Eq.35}$$

And the pressure drop is then calculated with

$$\Delta P_w = \frac{4000 f_w (L_t G_w^2)}{2 D_h \rho_w} \quad \text{Eq.36}$$

For the air side, in addition to previous parameters, coefficient of exit and entrance losses and the density at the exit need to be estimated. [26] This relation is described by the following

$$\sigma = {A_f}/{A_r}$$
$$K_e = (1-\sigma)^2 \quad \text{Eq.37}$$
$$K_c = 0.42(1-\sigma^2)^2$$

The friction factor and the pressure drop are then defined as [28]

$$f_a = {96}/{Re_a}$$
$$\Delta P_a = \left(\frac{G_a^2}{2\rho_a}\right)\left((1-\sigma^2+K_c) + \left(\frac{4 f_a L_c}{D_h}\right)\left(\frac{\rho_a}{\rho_{a_e}}\right) + 2\left(\frac{\rho_a}{\rho_{a_e}}\right) - (1-\sigma^2-K_e)\left(\frac{\rho_a}{\rho_{a_e}}\right)\right) \quad \text{Eq.38}$$

Table 11: Pressure drop values

ΔP results	Value	Unit
ΔP_a	515	Pa
ΔP_w	36.9	kPa

Pressure drop calculations are essential in terms of selection of the fans and the water pump to be used in the cooling system. This section will be discussed in the upcoming parts of this study. Pressure drop is function of friction properties which in return depends on Reynolds number and flow features. Air density, mass flux or in other words free flow area, loss coefficients and characteristic flow length are the other parameters defining pressure drop of the air side. [26] Apart from these, pressure drop is inversely proportional to the fluid density yet its effect on the heat rejection is quite little. [29]

4.1.1. Sensitivity Analysis

In order to see how the design reacts when assumed parameters and boundary conditions are changed, sensitivity analysis is going to be applied. These parameters are basically the essential parameters and the ones that characterizing the main parameters. Changes in mass flow rate, air outlet temperature, heat capacity ratio and radiator space requirements and their effects on heat rejected by radiator, are going to be investigated.

To start with the mass flow rate of both fluids, its effect on heat rejection is shown in Figure 18.

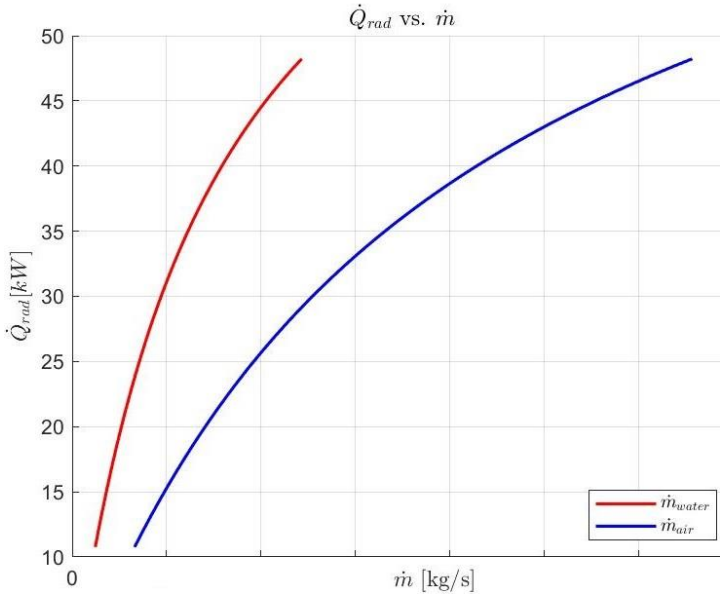

Figure 18: Mass flow rate effect

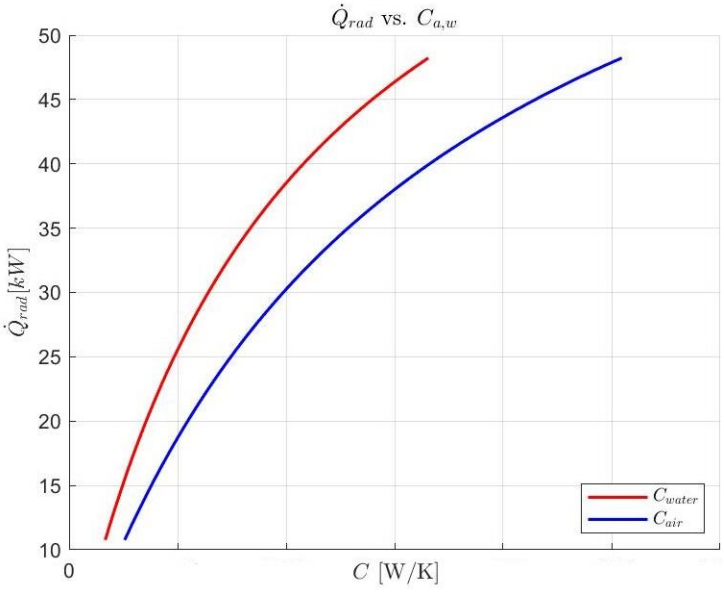

Figure 19: Specific heat capacity effect

It is observed that the increase in $\dot{m}_a$ and $\dot{m}_w$ is proportional to heat rejection rate of the radiator. This result is expected since heat rejection is a function of mass flow rate as it is shown in Eq.3.3.-12. Increase in $\dot{m}_w$ is more effective than of $\dot{m}_a$ and it can be explained by the fact that water has significantly higher thermal conductivity than air (See Table 6 and Table 7). It

is also observed that the required maximum heat rejection when the power requirements are at peak can be handled by the maximum flow rates of both fluids.

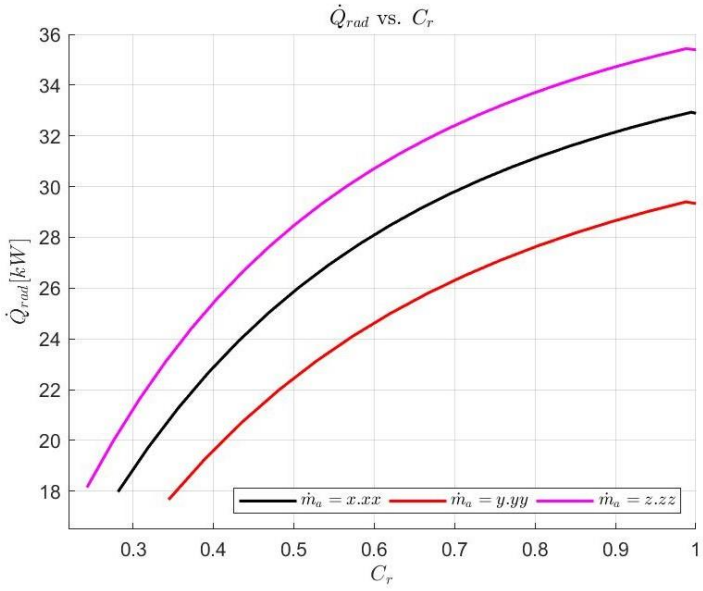

Figure 20: C_r when air flow is constant

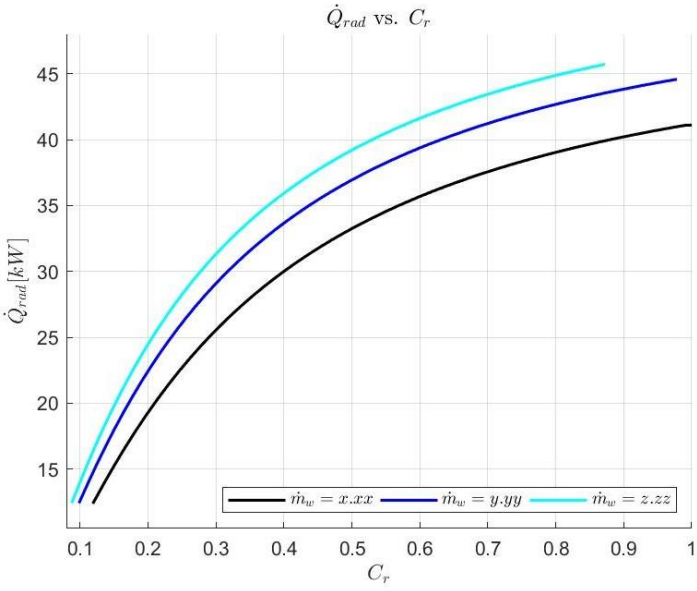

Figure 21: C_r when water flow is constant

Total heat capacity ratio is also an important parameter that needs to be investigated. To do so, following figures have been plotted. The reason why there are two plots are given in Figure 20 and Figure 21 is that to observe behavior of C_r, changes in $\dot{m}_a$ and $\dot{m}_w$ have to be observed independent of each other. Because C_r is a ratio between C_{min} and C_{max} and hence a ratio between $\dot{m}_a$ and $\dot{m}_w$ depending on which one is lesser in quantitiy. Observed behavior is expected and can be explained by increasing effect of mass flow rates on heat rejection rate. However, it is also seen that the increase only in water flow rate is not enough to satisfy high load operations of the FC module. In this radiator design, as flow rate of either fluid increases, flow rate of the other one increases too. Hence, the drawback is eliminated in reality yet still has to be considered in case the air flow rate has to be kept fixed.

As shown at the beginning of this section, air outlet temperature is given as a design criterion and as a range. So, a value is assumed within the range for the calculations and behavior of change in the assumed value is observed as shown in Figure 22.

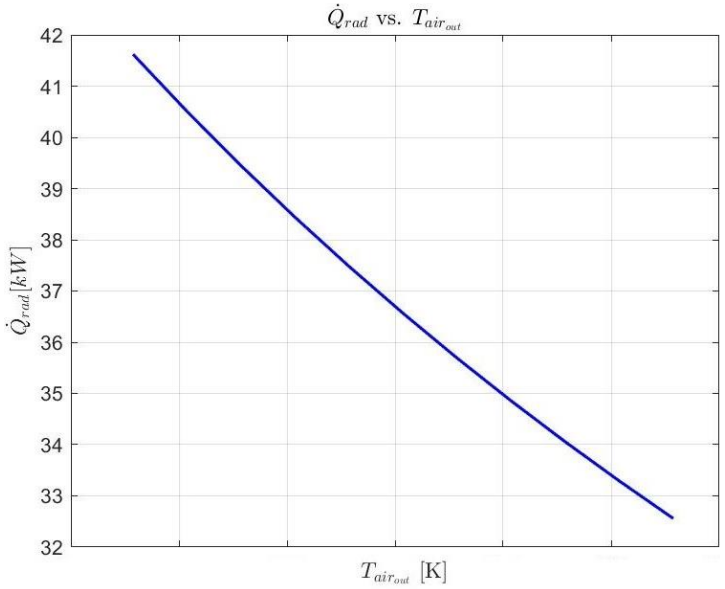

Figure 22: Air outlet temperature effect

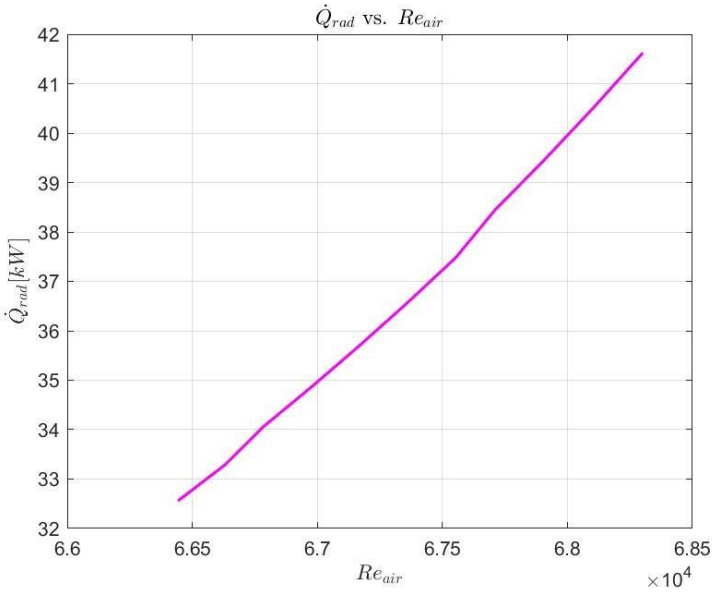

Figure 23: Re_a effect

It is also expected that change in assumed T_{a_o} will result in varying Re_a since parameters that characterizes Reynolds number strongly depends on average air temperature (See Eq.4.1.-24, 27). This resulting variations in Re_a are given in Figure 23.

Another important parameter that needs to be investigated is the dimensional assumptions made within the space limitations. As we know, surface area of the radiator is function of its height and length. Hence, effect of height and in return effect of area on the heat rejection rate is to be observed.

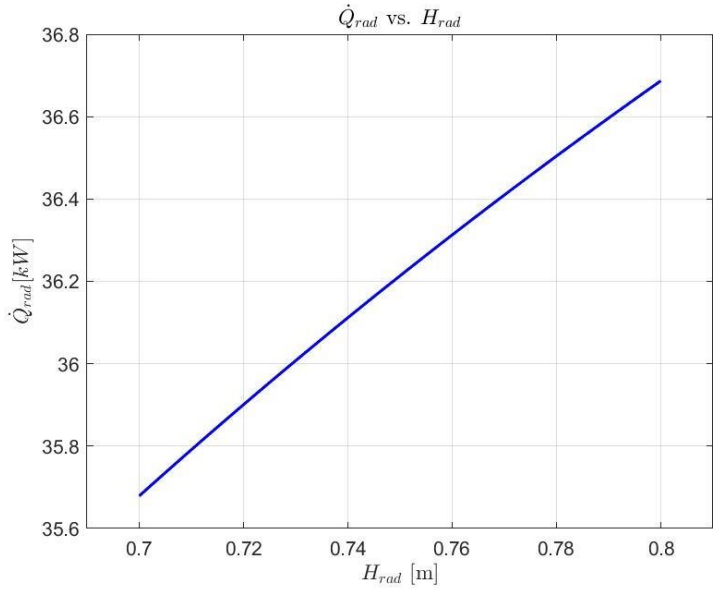

Figure 24: Effect of radiator height

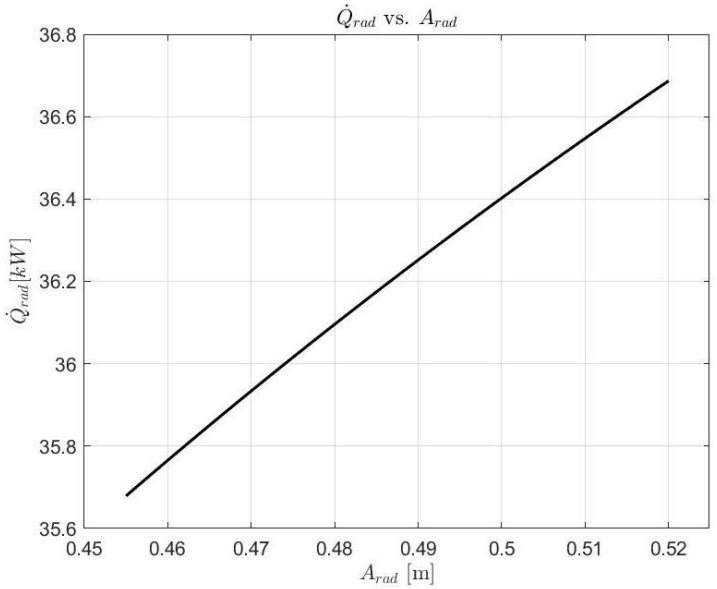

Figure 25: Effect of radiator area

As illustrated in Figure 24 and Figure 25, heat rejection rate increases almost linearly as height and hence, surface area of the radiator increases. This can be explained by the fact that, as the area that heat can interact with increases, amount of the heat being rejected increases as well. Eq.3.3.-10 explains this mathematically where $\dot{Q}_{cool}$ is a function of A_s.

4.2. Design Nº 2

The second design is a compact heat exchanger (CHE) design due to the fact that CHEs provide higher surface area of heat transfer per volume ratio. Hence, they are expected to occupy smaller area within a control volume. CHEs can be divided in two being finned-tube heat exchangers (FTHEs) and plate-fin heat exchangers (PFHEs).

The working principle of a CHE to be used in this design is similar to the one used in the first design in thermal and mechanical point of view. In this particular radiator, FTHE layout with circular tubes and continuous rectangular fins has been selected. Figure 26 can be referred for the schematic. The flow pattern of one fluid to another is the same as the first design, which is the crossflow arrangement where the flow of air and water are perpendicular to each other.

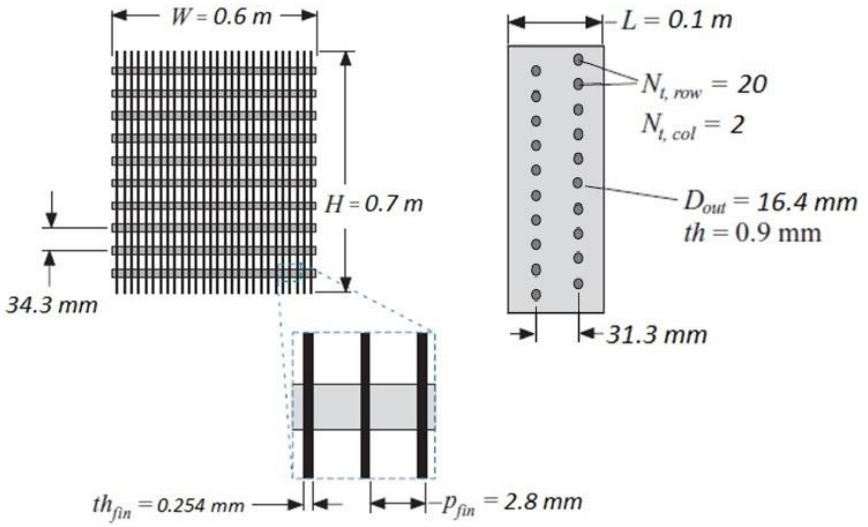

Figure 26: Schematic of radiator #2

Assumed radiator geometry and the tube dimensions are specified above and unlike the first design, copper is used as tube material instead of aluminum. Thus, much higher heat rejection from water is expected due to higher thermal conductivity of copper. Based on the evaluation from the calculations, results will be discussed in the following sections of this study. It should be noted that the assumed surface geometry for fins and tubes is selected from professor Kays' literature and designated as $CF - 7.0 - 58J$. [26]

LMTD method is used in this radiator design and the theory and methodology behind design steps will be discussed in the following parts of this section. The input parameters are given below in Table 12 where p_f refers to fin pitch and t_w stands for the tube wall thickness.

Table 12: Input parameters for design #2

Inputs	Value	Unit
L_r	100	mm
W_r	600	mm
H_r	700	mm
$D_{t,o}$	16.4	mm
t_w	0.9	mm
$N_{t,row}$	20	mm
$N_{t,col}$	2	mm
s_v	34.3	mm
s_h	31.3	mm
t_f	0.254	mm
p_f	2.8	mm
k_{cu}	394.7	W/mK

The water and air thermal properties are almost the same as the previous ones. However, for variability, another reference source has been used to derive the quantities from the thermodynamics tables [24]. These values are tabulated below in Table 13 and Table 14 respectively.

Table 13: Water thermal properties from Shah

Water Properties at average T_w		
ρ_w	979	kg/m^3
c_{p_w}	4185	J/kgK
k_w	0.66	W/mK
μ_w	$4.23x10^{-4}$	Pa/s
Pr_w	2.682	$[-]$

Table 14: Air thermal properties from Shah

Air properties at average T_a		
ρ_a	1.146	kg/m^3
c_{p_a}	1006	J/kgK
k_a	$2.77x10^{-2}$	W/mK
μ_a	$1.9x10^{-5}$	Pa/s
ν_a	$1.75x10^{-5}$	m^2/s
Pr_a	0.69	$[-]$

The way Prandtl number is obtained, either via thermodynamics tables or by calculating it, is the same as the one used in Eq.4-15.

Starting with the internal water flow through the tubes, there are some parameters to calculate. Non-dimensional numbers and eventually water side HTC require to know inner tube diameter and total tube length. These are given below

$$D_{t_i} = D_{t_o} - 2t_w$$
$$L_t = N_{t_{row}} N_{t_{col}} W \qquad \text{Eq.39}$$

Similar to the first design's relations, Reynolds number, Nusselt number and HTC are derived as given in Eq.4.1-24 and Eq.4.1-25 respectively. In CHEs, due to the compact design of the layers and tube surfaces, there occurs a dirt which we cannot neglect and have to take into account to obtain more accurate results at the end. First, the overall convective resistance on the water side is calculated. Then, the fouling resistance of the inner tube surfaces, which corresponds to aforementioned dirt resistance, is defined as shown below where the fouling factor is taken as $R''_{f,i} = 0.000175\, {}^{m^2K}/_{W}$ [26]

$$R_i = \frac{1}{\pi D_{t_i} L_t h_w}$$
$$R_{f_i} = \frac{R''_{f_i}}{\pi D_{t_i} L_t} \qquad \text{Eq.40}$$

Apart from the convection resistance; due to the copper tubes' conductivity, one needs to know conduction resistance as well. It is defined as [30]

$$R_{cond} = \frac{\ln\left(\frac{D_{t_o}}{D_{t_i}}\right)}{2\pi k_{cu} L_t} \qquad \text{Eq.41}$$

Air side heat transfer due to external flow is the next step to take in this design. To do so, geometrical parameters regarding the surfaces that the air is in contact with and the flow velocity need to be gathered. In order to find overall surface efficiency that will be used later on, total surface area of air side convection is required and that is the sum of the total area with and without fins. Corresponding relation is described as [30]

$$A_f = \frac{2W_r}{p_f}\left(H_r L_r - N_{t_{row}} N_{t_{col}} \pi \frac{D_{t_o}^2}{4}\right)$$
$$A_{uf} = \pi D_{t_o} L_t \left(1 - \frac{t_f}{p_f}\right) \qquad \text{Eq.42}$$

Hence, total surface area of air side yields

$$A_{a_{tot}} = A_f + A_{uf} \quad \text{Eq.43}$$

And the free flow area which will be used for the flow velocity of air is defined below

$$A_{ff} = W_r\left(H - N_{t_{row}} D_{t_o}\right)\left(1 - \frac{t_f}{p_f}\right) \quad \text{Eq.44}$$

The flow velocity is derived from Eq.47, similar to the one done during the first design.

$$u_a = {\dot{V}_a}/{A_{ff}} \quad \text{Eq.45}$$

Having derived the necessary quantities, Reynolds number, and corresponding HTC on the air side can be calculated as the way applied on the first design by using Eq.4.1-27 and Eq.4.1-29 respectively. However, due to having a turbulent flow in this case, the Nusselt number correlation used will differ and is given below [27]

$$Nu_w = 0.023\, Re_w^{0.8}\, Pr_w^{0.33} \quad \text{Eq.46}$$

Table 15 summarizes the obtained results so far.

Table 15: Obtained results

Parameter	Value	Unit
N_f	375	$[-]$
L_t	24	m
R_i	$5.4x10^{-5}$	${K}/{W}$
R_{f_i}	$1.2x10^{-4}$	${K}/{W}$
R_{cond}	$1.5x10^{-6}$	${K}/{W}$
Re_a	680.2	$[-]$
Re_w	$8.66x10^4$	$[-]$
Nu_a	65.16	$[-]$
Nu_w	388	$[-]$
h_a	109.8	${W}/{m^2K}$
h_w	$12.8x10^3$	${W}/{m^2K}$

According to the Reynolds numbers, air flow is significantly less effective when compared to water flow in terms of heat rejection. This leads to air side having a lesser Nusselt number and, hence, a smaller HTC than of the water side. However, specific thermal capacity of both fluids

is also important in that regard. When compared to the first radiator design, water side HTC is much higher, and this was an expected result. The reason is tubes are made of copper which has significantly higher thermal conductivity when compared to aluminum. Another reason is geometry of the tubes being used. Rather than flat tubes, circular tubes are selected.

In order to calculate the air resistance, fin efficiency and overall surface efficiency have to be derived. To do so, due to the different geometries used, another approach will be used in this design. η_f depends on characteristic length as it can be seen in Eq.4.1.-30 for the first design. Yet, in this case, L_c will be taken as effective fin radius. Then, the overall surface efficiency given as [30]

$$r_{f_{eff}} = \sqrt{\frac{A_f p_f}{2L_t\pi} + \frac{D_{t_o}^2}{4}}$$
$$\eta_o = 1 - A_f\left(\frac{1-\eta_f}{A_{a_{tot}}}\right) \qquad \text{Eq.47}$$

Having derived all the required parameter, convective air resistance then can be calculated by using the correlation below

$$R_o = \frac{1}{\eta_o h_a A_{a_{tot}}} \qquad \text{Eq.48}$$

The next step is to find the total conductance which is the inverse of sum of all the resistances that have been derived so far. Correlation regarding total conductance is defined as follows

$$UA = \frac{1}{R_{tot}} = \frac{1}{R_i + R_{f_i} + R_{cond} + R_o} \qquad \text{Eq.49}$$

As mentioned previously, LMTD method is applied on this design's calculations. Recalling Eq.3.3.-10, it is seen that correction factor has to be estimated as well. This correction factor is due to the crossflow arrangement of the CHE. Effectiveness factor and capacitance ratio factors need to be calculated and then the resulting correction factor has to be estimated by using the heat exchanger maps [26]. These factors are defined as

Eq.50

$$T_{a_o} - T_{a_i}$$

$$R_{CF} = \frac{T_{w_i} - T_{w_o}}{T_{a_o} - T_{a_i}}$$

By using the HE maps from the textbook of professor Kays, correction factor is obtained as $CF = 0.92$. After obtaining LMTD and the correction factor, heat rejection rate by the radiator is calculated (See Eq.3.3.-10). Similarly, the outlet temperatures of both fluids are found by the same correlation which were used for the first radiator in Section 4.1.

Table 16: Major results

Parameter	Value	Unit
$\boldsymbol{\eta_f}$	0.88	$[-]$
$\boldsymbol{\eta_o}$	0.89	$[-]$
$\boldsymbol{R_o}$	$3.2x10^{-2}$	W/K
$\boldsymbol{CF}$	0.92	$[-]$
$\boldsymbol{LMTD}$	19	K
$\boldsymbol{UA}$	≈ 2100	W/K
$\boldsymbol{T_{a_o}}$	55.86	℃
$\boldsymbol{T_{w_o}}$	58.91	℃
$\boldsymbol{\dot{Q}_{rad}}$	39	kW

Similar to the first design's results, obtained exit temperatures are within the acceptable range upon company requirements and manufacturer specifications. Both air and water outlet temperatures differ less than order of magnitude from the ideal temperatures. The main difference what makes CHE design preferable is that it satisfies required heat rejection (See Table 4). Furthermore, it can reject more heat with smaller volume occupied (See Table 12).

The theory and methodology to obtain the pressure drops slightly differ in terms of geometrical properties yet the correlations are almost identical to the ones used for the first design. Hence, there are new parameters to be defined, effective channel width, which in return will be used to obtain its hydraulic diameter that is equal to the heat transfer diameter. These are given in equation below.

$$W_{ch} = \frac{W_r - N_f t_f}{N_f}$$

$$D_{h_{ch}} = W_{ch} \frac{H_r}{2(W_{ch} + H_r)} \qquad \text{Eq.51}$$

Having obtained the hydraulic diameter, the pressure drops are calculated by using the approach given in Eq.4.1-37 and Eq.4.1.-39. Results of the pressure drop are given below in Table 17.Table 16

Table 17: Pressure drop values

Parameter	Value	Unit
f_a	0.1	$[-]$
f_w	0.02	$[-]$
ΔP_a	187.1	Pa
ΔP_w	70.02	kPa

Results above are acceptable in terms of manufacturer specifications. Pressure drop highly depends on flow density and HTC. Thus, change in these parameters as well as geometrical properties and friction factor, will yield different results which in turn may affect the design criteria of the fan and pump. [29]

4.2.1. Sensitivity Analysis

The same procedure applied to first radiator is now to be implemented on the second one as well. The parameters that are intended to be investigated are the same as of the first radiator. Figure 27 and Figure 28 show the behavior of the mass flow rates and specific heat capacities.

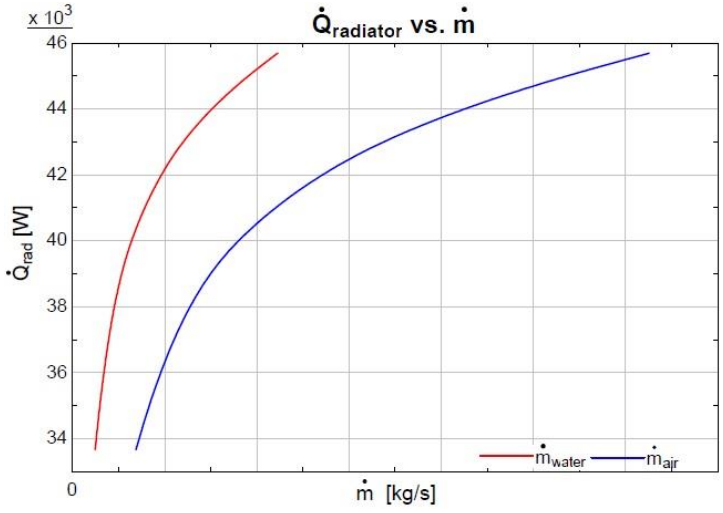

Figure 27: Effect of mass flow rate

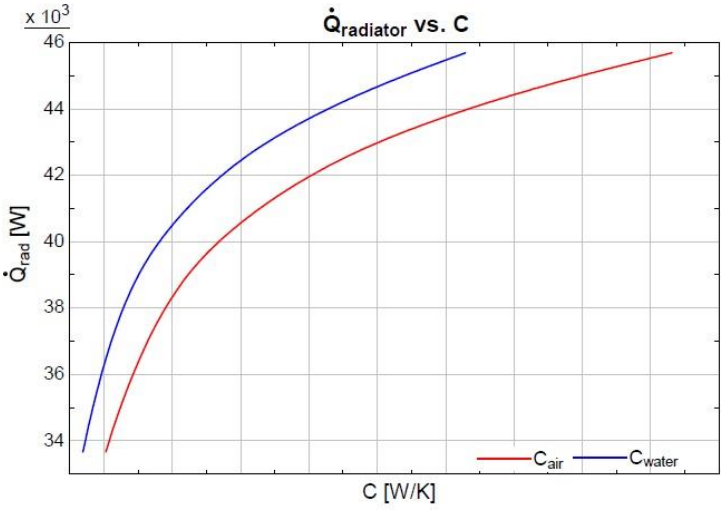

Figure 28: Effect of specific heat capacity

Similar to the previous results, mass flow rate and rate of heat rejection are observed to be proportional to each other. proportional to heat rejection rate of the radiator. It is also seen that the increase in mass flow rate of water is more effective since higher heat rejection rates are

obtained with less percentage increase. As it was in previous design, maximum heat rejection under peak power requirements can be handled by the current radiator as well.

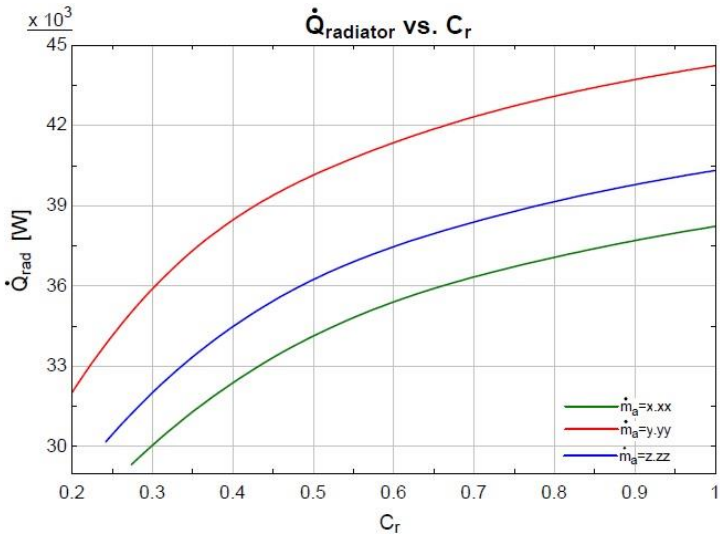

Figure 29: C_r when air flow is constant

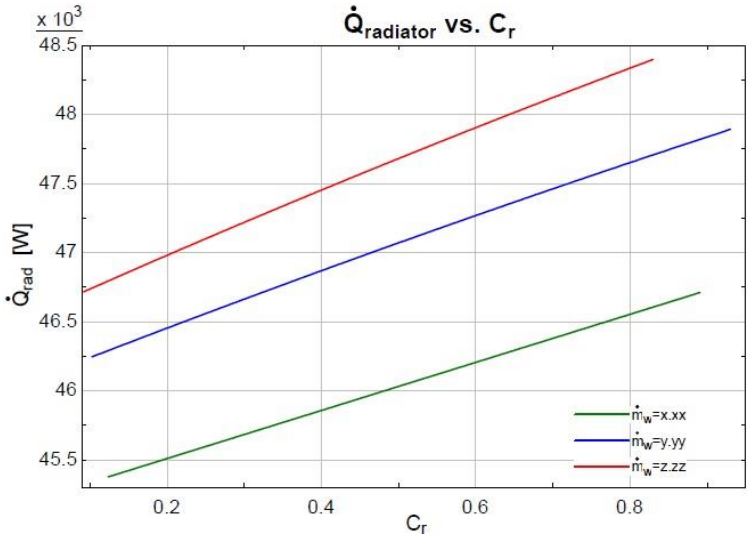

Figure 30: C_r when water flow is constant

The approach and methodology behind investigating the total heat capacity ratio is as the same as the one applied for the previous radiator. To observe behavior of C_r, changes in $\dot{m}_a$ and $\dot{m}_w$ have to be observed independent of each other. Because C_r is a ratio between C_{min} and C_{max} and hence a ratio between $\dot{m}_a$ and $\dot{m}_w$ depending on which one becomes minimum and maximum. Another result that is derived out of the plots above is that unlike the previous design, individual increases of mass flow rates of both fluids is satisfactory to handle high load operations of the FC module. This situation is achieved when the maximum possible flow rates are delivered. It is also observed that when the air flow is fixed at a higher amount, achievable heat rejection rate with the same C_r becomes higher. This is the same when the water flow is kept constant at a higher amount as well. According to the initial conditions, change in flow rate of one fluid affects the flow rate of the other one in the same way. Hence, even if the flow rate were not compensating high load operation conditions, it wouldn't be a fatal problem in real application of the radiator. However, since this radiator can achieve design requirements with changes in either fluid's mass flow rates, possibility of not being able to deliver the maximum power is eliminated.

As it was in previous section, air outlet temperature is given as a design criterion in form of a range. Response obtained from heat rejection rate in dependence of the outlet temperature is provided in Figure 31.

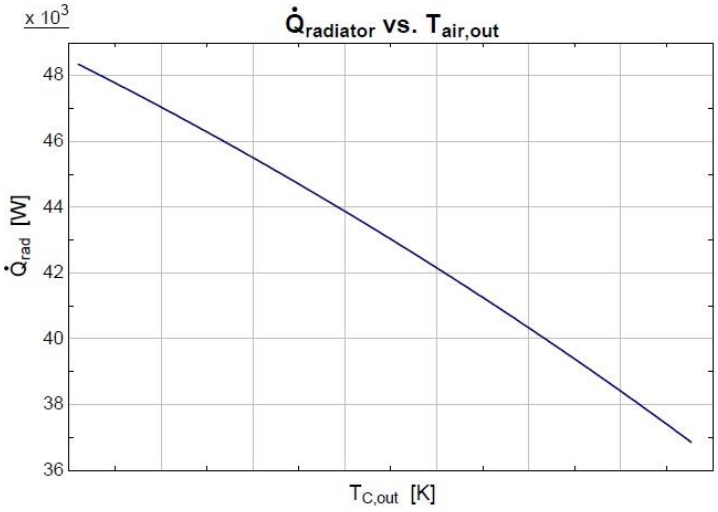

Figure 31: Air outlet temperature

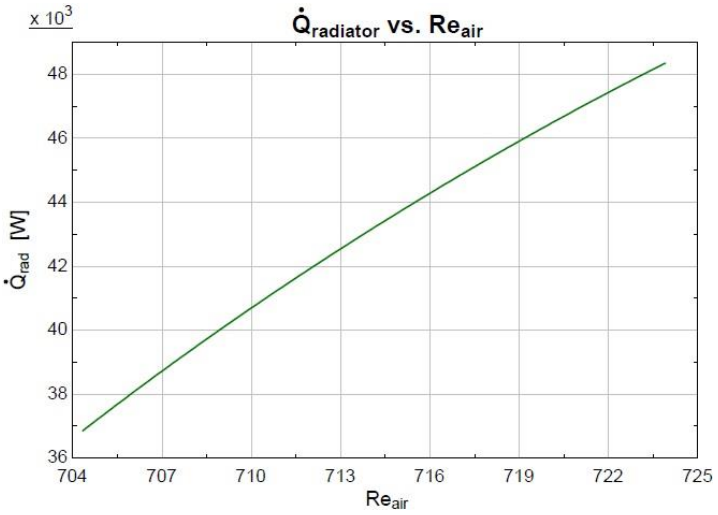

Figure 32: Effect of Re_a

Due to the varying temperature, parameters that characterizes Reynolds number will also vary and it will lead to change in Reynolds number of air itself. This behavior of Re_a is shown in Figure 32.

Regarding the effect of radiator height and corresponding surface area on the heat rejection rate is also investigated. The obtained results are more or less the same as of the previous radiator.

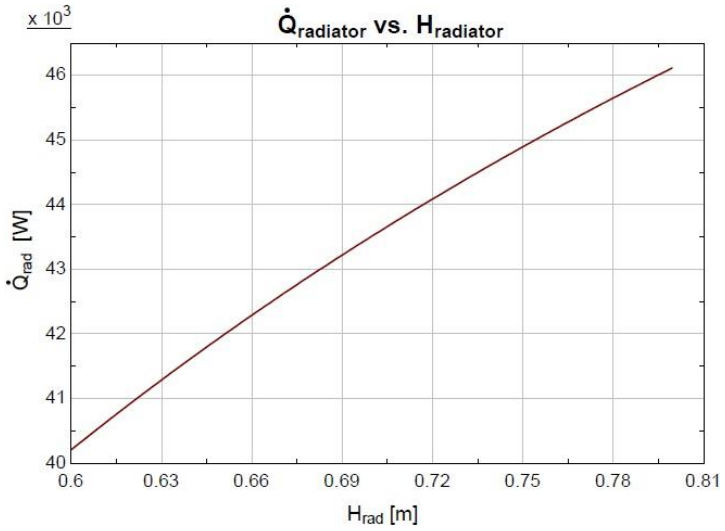

Figure 33: Effect of radiator height

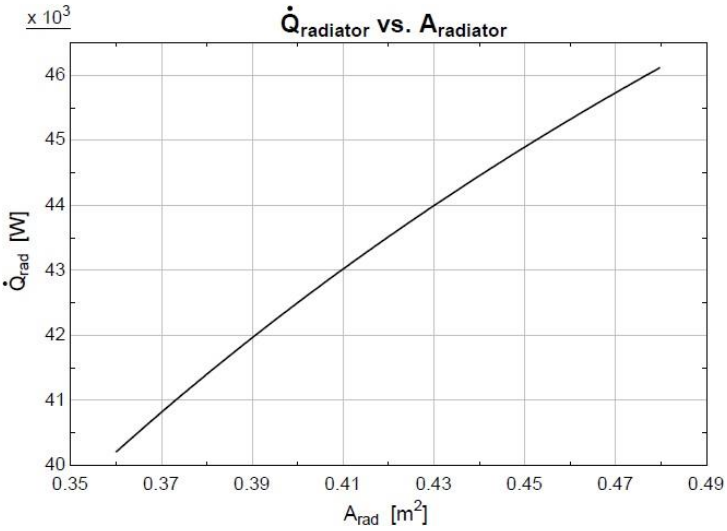

Figure 34: Effect of radiator area

As Figure 33 and Figure 34 above show, heat rejection rate increases almost linearly as height and due to being a function of height, surface area of the radiator increases either. Again, it is be explained by the fact that, as the area that heat can interact with increases, amount of the heat being rejected increases as well.

4.3.Fan

For the fan selection, what needs to be known are the pressure drop on the air side and its volumetric flow rate under mean operating conditions. Pressure drop for both designs have been derived in the previous sections of this study and volumetric flow rate is known from the manufacturer specifications and the company requirements. Another selection criterion is the operating temperature. However, either fan types allow a wide range of temperature and assumed ambient temperature is within this range for both cases. Since required values are known, suitable fans can be selected from a recognized manufacturer catalogue. For this study, SPAL Automotive Srl has been taken as reference. [31]

In the market, there are two different types of fans that can be chosen. These are brushed and brushless fans. Brushed fans require maintenance and can be dangerous in case there occurs spark due to leakage of hydrogen or coolant. However, they are cost effective. On the other hand, with brushless fans, this danger is eliminated. Moreover, they have a longer lifetime and the same fan output can be obtained by a smaller fan diameter which is essential if the space requirements are strict just like in this study.

In accordance with the explained methodology, suitable fans are tabulated below in Table 18.

Table 18: Fan selection for the first radiator

Fan type	Model	N⁰ of fans	Diameter [mm]
Brushed	VA18-BP71/LL-86A	2	385
Brushless	VA113-BBL504P/N-94A	2	305

Using a FC module working with hydrogen, and other aforementioned advantages, brushless fans are recommended in this design. The performance diagram of the recommended fan is given below in Figure 35. [31]

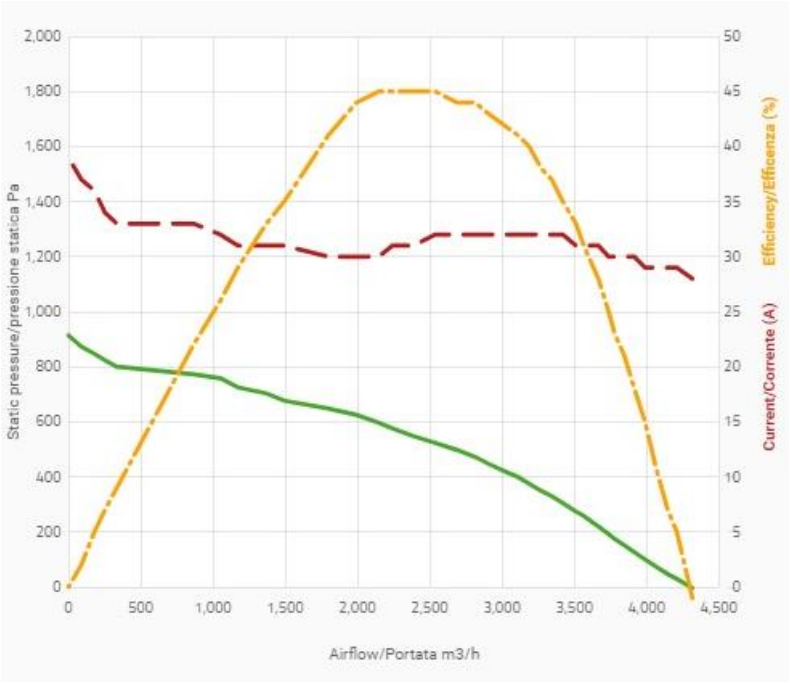

Figure 35: Brushless VA113-BBL504P/N-94A

The specifications of the fan, including fan speed, supply voltage and weight, will later be provided in the appendix section of this report.

Regarding the second radiator, the methodology applied is the same as the one of the first radiator. The same manufacturer has been taken as reference. Among the fans available on the catalogue, second design can use more options due to having less pressure drop on the air side. This will also allow us to select a fan with a smaller diameter, for both brushed and brushless option, which is good because second radiator has a smaller surface area on which the selected fans can be mounted. Table 19 below shows the results from the fan selection. [31]

Table 19: Fan selection for the second radiator

Fan type	**Model**	**Nº of fans**	**Diameter [mm]**
Brushed	VA01-BP90/LL-79S /	2	305
	VA01-BP90/LL-66A	2	305
Brushless	VA89-BBL338P/N-94A	2	305

It should be mentioned that any fan having a diameter of 305 mm can be selected among the list of brushless fans in the catalogue. However, the one with the most capability of airflow is selected for the simplicity and the performance diagram of it is provided in Figure 36.

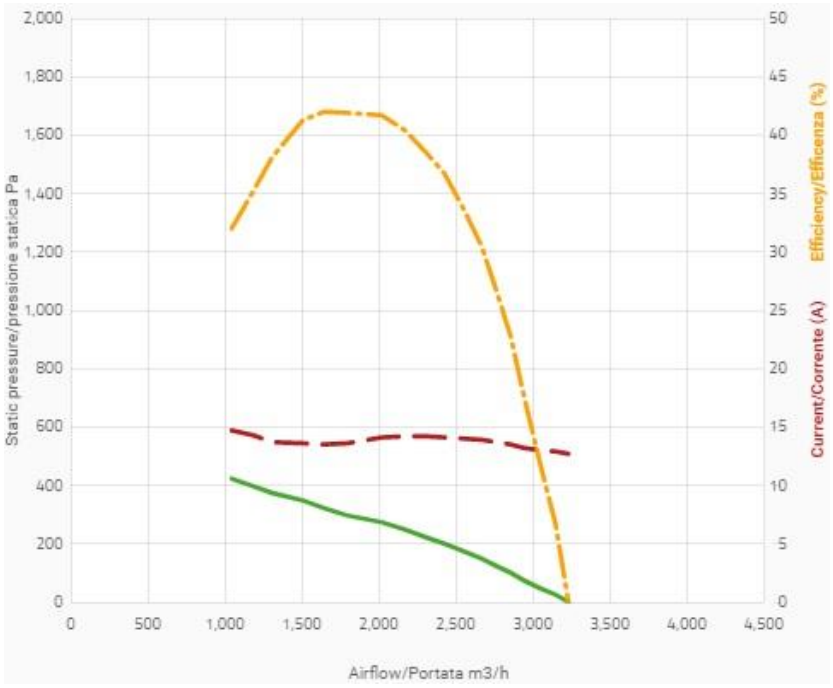

Figure 36: Brushless VA89-BBL338P/N-94A

Similar to the selected fan for the first radiator, specifications of this model is also available in the appendix section of this report.

4.4.Pump

The pump requirements strongly depend on the coolant flow rate and the pressure drop characteristics. When the pressure difference across the control volume changes, coolant flow rate will change as well. Pressure drop results obtained from both designs discussed in sections 4.1 and 4.2 are acceptable since the results are within the range which varies from 50-120 kPa for similar applications [32].

From the initial design conditions and from the calculated parameters, coolant volumetric flow rate and water side pressure drops are known. Thus, parameters needed to be known for the pump selection have been obtained.

Table 20: Pump selection for both radiators

		

Model	DHC-200 (200W)	PMP-850 (200W)
Controller	CAN, On/Off type	CAN, On/Off type
Capacity	45LPM / 1bar / 12V	45LPM / 1bar / 12V

Table 20 above shows the selected pump's parameters. Either of the selected fans satisfy the requirements for both radiators designed which are explained in previous sections. Japanese manufacturer GMB has been taken as a reference for the pump selection [33]. These pumps provided above are electric water pumps which are widely being used in hybrid, electric and FC applications. Furthermore, apart from being less heavy, they provide noise reduction and significant durability which in return result in higher efficiency [33]. This sort of water pumps are equipped with brushless DC motors which are also used in brushless fans as discussed in section 4.3.

4.5. Cooling Power

The assessment of the cooling power consists of hydraulic losses and transferred heat fluxes [29]. Transferred heat is the heat rejected by the radiator to keep the FC module under operating temperatures. Hydraulic losses are divided into two being the losses due to fan and the losses due to pumping the coolant. In order to calculate the cooling power, power dissipated by the fan and the pump have to be known. Below in Eq.4.5.-53, correlations to calculate these parameters are given [34].

$$P_{fan} = \frac{\dot{V}_a \Delta P_a}{\eta_{fan}}$$
$$P_{pump} = \frac{\dot{V}_w \Delta P_w}{\eta_{pump}} \qquad \text{Eq.52}$$

Power consumed by the fan and pump operation are both functions of pressure drop, volumetric flow rate and efficiency of the related device. Volumetric flow rate and pressure drop for air and water have been given and calculated in previous sections of this study. Fan efficiencies of designed radiators can be obtained from specification sheets or performance charts (See Figure 35 and Figure 36). Regarding the efficiency of the electric water pump, its value varies between 0.7 and 0.9 [32]. To be on the safety side, the lowest values have been used in the calculations. In accordance with these, after all, the cooling power is evaluated as

$$P_{cooling} = \dot{Q}_{rad} + 2P_{fan} + P_{pump} \quad \text{Eq.53}$$

Below in Table 21 fan efficiencies, power consumed by fan and pump, as well as the cooling power for both radiators have been presented.

Table 21: Cooling power

	Radiator #1	**Radiator #2**	**Unit**
$\boldsymbol{\eta_{fan}}$	0.45	0.4	$[-]$
$\boldsymbol{\eta_{pump}}$	0.7	0.7	$[-]$
$\boldsymbol{P_{fan}}$	1800	770	$[W]$
$\boldsymbol{P_{pump}}$	36	63	$[W]$
$\boldsymbol{P_{cooling}}$	38.6	40.2	$[kW]$

The main reason why the power consumed by the fan in the first design is greater than the one in the second design is simply having larger pressure drop on the air side. Similarly, having larger pressure drop on the water side makes the power consumed by the pump in the second radiator higher than of the first one.

5. Conclusion

Fuel cell systems are widely used and quite applicable in automotive applications, as well as being able to be used as a stationary power source. In order to FC systems under operating temperatures requires a successful cooling system design including its heat exchanger, fan and pump.

Firstly, two different layouts have been selected for the radiator in accordance with the design limitations. Thermal properties of water and air have been derived and calculated based on the temperatures of both fluids. Results for the first radiator, with aluminum flat tubes and rectangular fins, yield that $36.7\,kW$ of heat is rejected by occupying volume of $0.1x0.65x0.8\,m^3$. The second radiator, on the other hand, is capable of rejecting $39\,kW$ of heat in a space of $0.1x0.6x0.8$. It is shown that the second radiator is more efficient since higher heat rejection is obtained with less space occupied.

Secondly, previously calculated pressure drops, and volumetric flow rates have been used to select fan and pump for each design. The pump selected is suitable to both designs. Regarding the fan, it is recommended to use brushless fan due to having a higher efficiency, lifespan and not being a thread in case of hydrogen leakage. Another reason for this selection is that, a

smaller fan can be used for the first radiator which occupies smaller space and allows flexibility in the design and for further optimizations.

Afterwards, cooling power of both radiators is calculated, and the second radiator consumes more power for cooling since electric energy is greater. This is expected due to having higher heat rejection capacity even though sum of the losses in fan and pump are smaller when compared to the first radiator.

Despite being more advantageous, the second radiator is designed with coated copper tubes instead of aluminum ones that were selected in the first radiator. This will result in increased cost and it may be considered as a drawback.

To sum up, both radiators are explained including the methodology behind them and their analysis have been implemented and provided. As future work, more analysis can be made to optimize radiators and different tube and fin materials can be tried. Moreover, another fluid with higher specific heat and thermal capacities can be used as coolant.

References

[1] J. M. Plc, Fuel Cell Today Limited, 2020. [Online]. Available: http://www.fuelcelltoday.com/about-fuel-cells/benefits. [Accessed March 2020].

[2] C. Spiegel, Designing and Building Fuel Cells, McGraw-Hill, 2007.

[3] A. University, "Department Of Energy Technology," Aalborg University, 2019.

[4] FCHEA, "Fuel Cell & Hydrogen Energy Association," [Online]. Available: http://www.fchea.org/fuelcells. [Accessed 2020].

[5] R. N. Castellano, Alternative Energy Technologies: Opportunities and Markets, 2012.

[6] U. D. o. E. H. Program, October 2006. [Online]. Available: https://www.hydrogen.energy.gov/. [Accessed March 2020].

[7] S. Institution, "https://americanhistory.si.edu/," 2017. [Online]. Available: https://americanhistory.si.edu/fuelcells/basics.htm. [Accessed 2020].

[8] Ö. Çamcı, "Application of Fuel Cell in Motor Vehicles," Yıldız Technical University Institute of Science, 2005.

[9] Akbulut, "Fuel Cell Hybrid Plants," Fırat University Institute of Science, 2007.

[10] E. W. B. S. B. S. S. V. Hacker, Carbon nanofiber-based active layers for fuel cell cathodes – preparation and characterization, Elsevier, 2005.

[11] C. E. Inc., Cadex, 2003-2018. [Online]. Available: https://batteryuniversity.com/. [Accessed 2020].

[12] F. Barbir, PEM Fuel Cells Theory and Practice, Elsevier, 2012.

[13] M. Secanell, "Computational modeling and optimization of proton exchange membrane fuel cells," University of Alberta, 2007.

[14] D. s.r.o., "DEVINN," 2014. [Online]. Available: https://www.devinn.cz/en/.

[15] W. &. S. X. &. N. H. Yu, "Air Compressors for Fuel Cell Vehicles: An Systematic Review," *SAE International Journal of Alternative Powertrains,* vol. 4, May 2015.

[16] A. D. F. Solutions, "AMETEK," 2015. [Online]. Available: https://www.ametekdfs.com/learningzone/whitepapers/selectingtherightblowrandpumpforfuelcellapplications.

[17] Mann+Hummel, "The Mann+Hummel Group," 2020. [Online]. Available: https://oe-products.mann-hummel.com/en/applications/fuel-cells/.

[18] F. K. M. B. A. K. a. A. M. D. Rezzak, "A DC-DC converter-based PEM fuel cell system emulator," *2011 International Conference on Power Engineering, Energy and Electrical Drives,* 2011.

[19] M. H. Bargal, M. A. Abdelkareem, Q. Tao, J. Li, J. Shi and Y. Wang, "Liquid cooling techniques in proton exchange membrane fuel cell stacks: A detailed survey," *Alexandria Engineering Journal,* 2020.

[20] R. T. Ashley Fly, "A comparison of evaporative and liquid cooling methods for fuel cell vehicles.," 2016. [Online]. Available: https://hdl.handle.net/2134/21933.

[21] C. Spiegel, PEM Fuel Cell Modelling and Simulation Using MATLAB, Elsevier, 2008.

[22] D. Prof. Ing. Jan Macek, "FC PEM Model for Compressor Assignment and Overall Optimization," Praha, 2020.

[23] A. T. A. F. M. R. K. S. L. Magistri, "Heat Exchangers for Fuel Cell and Hybrid System Applications," *3rd International Conference on Fuel Cell Science, Engineering and Technology,* May 2006.

[24] R. K. S. a. D. P. Sekulic, Fundamentals of Heat Exchanger Design, Rochester, New York: John Wiley & Sons, Inc., 2003.

[25] T. B. A. L. F. Incropera, Fundamentals of Heat and Mass Transfer 8th Ed., University of California, Los Angeles: WILEY.

[26] A. W.M.Kays, Compact Heat Exchangers, McGraw-Hill, 1964.

[27] D. Prof. Ing. Jan Macek, "Lecture: Convection," 2014.

[28] O. C. Jones Jr., "An Improvement in the Calculation of Turbulent Friction in Rectangular Ducts," *Journal of Fluid Engineering,* no. ASME, 1976.

[29] D. Prof. Ing. Jan Macek, "Lecture: Engine Cooling Systems and Heat Exchangers," 2014.

[30] S. K. Gregory Nellis, Heat Transfer, Cambridge University Press, 2008.

[31] S. A. Srl, SPAL Automotive Srl, [Online]. Available: https://www.spalautomotive.it/. [Accessed 05 2020].

[32] T. Lahvic, Investigation of engine heat rejection, Ford Motor Co, 1986.

[33] G. C. Japan, "GMB," 2020. [Online]. Available: https://www.gmb.jp/en/product/cooling/e_water_pump.html.

[34] P. O. A. G.-R. J. N. A.J. Torregrosa, "A Methodology for the Design of Engine Cooling Systems in Standalone Applications," SAE International, 2010.

[35] D. G. B. L. A. M. a. X. F. Matthew Carl, "The Theoretıcal And Experımental Investıgatıon Of The Heat Transfer Process Of An Automobıle Radıator," ASEE Gulf Southwest Annual Conference, Beaumont, TX 77710, 2012.

APPENDIX

Fan VA113-BBL504P/N-94A

01/07/2020

BRUSHLESS AXIAL FANS

VA113-BBL504P/N-94A

Performance diagram

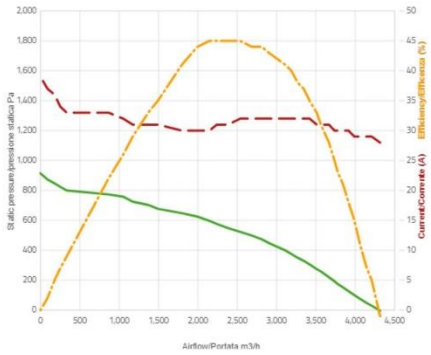

Pressure: 1 Pa = 0,004 inH2O Airflow: 1 m3/h = 0.59 cfm

Features

Max fan speed	rpm	4750
Min fan speed	rpm	1200
Sound pressure level	dBA	85,6 - at 1 m
Weight	kg	2,60
Operating supply voltage range	V	16 .. 32 at the Drive Connector
Supply voltage to reach max speed	V	26 .. 32 at the Drive Connector
Operating ambient temperature range	°C	-40 .. +110
Speed derating threshold	°C	+65 (*)
Storage temperature range	°C	-40 .. +125

SPAL Automotive s.r.l. via per Carpi 26/B 42015 Correggio IT REG.IMP CF e PIVA IT01755790357

Max fan speed	rpm	4750
Lifetime	h	up to 40000 hours depending on mission profile
Time from 0 rpm to max speed	s	10
Load dump protection (Pulse 5b)	V	65 - Pulse peak voltage (Us*) - ISO16750 - 2:2010
Reverse polarity protection		ISO 16750-1 functional status class C - device fully functional after connecting the polarity
Notes(*): Few minutes ambient temperature transients do not engage the derating owing to the thermal inertia of the system. Overloads may anticipate derating.		

Fan VA89-BBL338P/N-94A

01/07/2020

BRUSHLESS AXIAL FANS

VA89-BBL338P/N-94A

Performance diagram

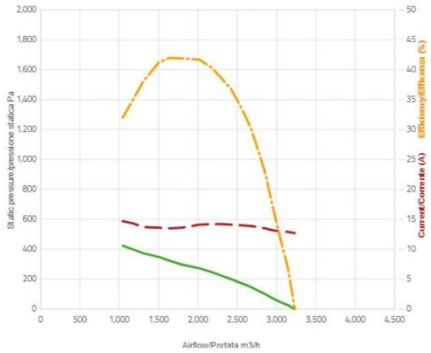

Pressure: 1 Pa = 0,004 inH2O Airflow: 1 m3/h = 0.59 cfm

Features

Max fan speed	rpm	3650
Min fan speed	rpm	900
Sound pressure level	dBA	78 - at 1 m
Weight	kg	2,20
Operating supply voltage range	V	16 .. 32 at the Drive Connector
Supply voltage to reach max speed	V	26 .. 32 at the Drive Connector
Operating ambient temperature range	°C	-40 .. -95
Speed derating threshold	°C	+85 (*)
Storage temperature range	°C	-40 .. +120

SPAL Automotive s.r.l. via per Carpi 26/B 42015 Correggio IT REG.IMP CF e PIVA IT01755790357

Max fan speed	rpm	3650
Lifetime	h	up to 40000 hours depending on mission profile
Time from 0 rpm to max speed	s	15
Load dump protection (Pulse 5b)	V	65 - Pulse peak voltage (Us*) - ISO16750 - 2:2010
Reverse polarity protection		ISO 16750-1 functional status class C - device fully functional after connecting the polarity
Notes(*): Few minutes ambient temperature transients do not engage the derating owing to the thermal inertia of the system. Overloads may anticipate derating.		

Thermophysical Properties of Matter [25]

TABLE A.4 Thermophysical Properties of Gases at Atmospheric Pressure[a]

T (K)	ρ (kg/m^3)	c_p (kJ/kg · K)	$\mu \cdot 10^7$ (N · s/m^2)	$\nu \cdot 10^6$ (m^2/s)	$k \cdot 10^3$ (W/m · K)	$\alpha \cdot 10^6$ (m^2/s)	Pr
Air, M = 28.97 kg/kmol							
100	3.5562	1.032	71.1	2.00	9.34	2.54	0.786
150	2.3364	1.012	103.4	4.426	13.8	5.84	0.758
200	1.7458	1.007	132.5	7.590	18.1	10.3	0.737
250	1.3947	1.006	159.6	11.44	22.3	15.9	0.720
300	1.1614	1.007	184.6	15.89	26.3	22.5	0.707
350	0.9950	1.009	208.2	20.92	30.0	29.9	0.700
400	0.8711	1.014	230.1	26.41	33.8	38.3	0.690
450	0.7740	1.021	250.7	32.39	37.3	47.2	0.686
500	0.6964	1.030	270.1	38.79	40.7	56.7	0.684
550	0.6329	1.040	288.4	45.57	43.9	66.7	0.683
600	0.5804	1.051	305.8	52.69	46.9	76.9	0.685
650	0.5356	1.063	322.5	60.21	49.7	87.3	0.690
700	0.4975	1.075	338.8	68.10	52.4	98.0	0.695
750	0.4643	1.087	354.6	76.37	54.9	109	0.702
800	0.4354	1.099	369.8	84.93	57.3	120	0.709
850	0.4097	1.110	384.3	93.80	59.6	131	0.716
900	0.3868	1.121	398.1	102.9	62.0	143	0.720
950	0.3666	1.131	411.3	112.2	64.3	155	0.723
1000	0.3482	1.141	424.4	121.9	66.7	168	0.726
1100	0.3166	1.159	449.0	141.8	71.5	195	0.728
1200	0.2902	1.175	473.0	162.9	76.3	224	0.728
1300	0.2679	1.189	496.0	185.1	82	257	0.719
1400	0.2488	1.207	530	213	91	303	0.703
1500	0.2322	1.230	557	240	100	350	0.685
1600	0.2177	1.248	584	268	106	390	0.688
1700	0.2049	1.267	611	298	113	435	0.685
1800	0.1935	1.286	637	329	120	482	0.683
1900	0.1833	1.307	663	362	128	534	0.677
2000	0.1741	1.337	689	396	137	589	0.672
2100	0.1658	1.372	715	431	147	646	0.667
2200	0.1582	1.417	740	468	160	714	0.655
2300	0.1513	1.478	766	506	175	783	0.647
2400	0.1448	1.558	792	547	196	869	0.630
2500	0.1389	1.665	818	589	222	960	0.613
3000	0.1135	2.726	955	841	486	1570	0.536

TABLE A.6 Thermophysical Properties of Saturated Water[a]

Temperature, T (K)	Pressure, p (bar)[b]	Specific Volume (m^3/kg) $v_f \cdot 10^3$	Specific Volume (m^3/kg) v_g	Heat of Vaporization, h_{fg} (kJ/kg)	Specific Heat (kJ/kg · K) $c_{p,f}$	Specific Heat (kJ/kg · K) $c_{p,g}$	Viscosity ($N \cdot s/m^2$) $\mu_f \cdot 10^6$	Viscosity ($N \cdot s/m^2$) $\mu_g \cdot 10^6$	Thermal Conductivity (W/m · K) $k_f \cdot 10^3$	Thermal Conductivity (W/m · K) $k_g \cdot 10^3$	Prandtl Number Pr_f	Prandtl Number Pr_g	Surface Tension, $\sigma_f \cdot 10^3$ (N/m)	Expansion Coefficient, $\beta_f \cdot 10^6$ (K^{-1})	Temperature, T (K)
273.15	0.00611	1.000	206.3	2502	4.217	1.854	1750	8.02	569	18.2	12.99	0.815	75.5	−68.05	273.15
275	0.00697	1.000	181.7	2497	4.211	1.855	1652	8.09	574	18.3	12.22	0.817	75.3	−32.74	275
280	0.00990	1.000	130.4	2485	4.198	1.858	1422	8.29	582	18.6	10.26	0.825	74.8	46.04	280
285	0.01387	1.000	99.4	2473	4.189	1.861	1225	8.49	590	18.9	8.81	0.833	74.3	114.1	285
290	0.01917	1.001	69.7	2461	4.184	1.864	1080	8.69	598	19.3	7.56	0.841	73.7	174.0	290
295	0.02617	1.002	51.94	2449	4.181	1.868	959	8.89	606	19.5	6.62	0.849	72.7	227.5	295
300	0.03531	1.003	39.13	2438	4.179	1.872	855	9.09	613	19.6	5.83	0.857	71.7	276.1	300
305	0.04712	1.005	29.74	2426	4.178	1.877	769	9.29	620	20.1	5.20	0.865	70.9	320.6	305
310	0.06221	1.007	22.93	2414	4.178	1.882	695	9.49	628	20.4	4.62	0.873	70.0	361.9	310
315	0.08132	1.009	17.82	2402	4.179	1.888	631	9.69	634	20.7	4.16	0.883	69.2	400.4	315
320	0.1053	1.011	13.98	2390	4.180	1.895	577	9.89	640	21.0	3.77	0.894	68.3	436.7	320
325	0.1351	1.013	11.06	2378	4.182	1.903	528	10.09	645	21.3	3.42	0.901	67.5	471.2	325
330	0.1719	1.016	8.82	2366	4.184	1.911	489	10.29	650	21.7	3.15	0.908	66.6	504.0	330
335	0.2167	1.018	7.09	2354	4.186	1.920	453	10.49	656	22.0	2.88	0.916	65.8	535.5	335
340	0.2713	1.021	5.74	2342	4.188	1.930	420	10.69	660	22.3	2.66	0.925	64.9	566.0	340
345	0.3372	1.024	4.683	2329	4.191	1.941	389	10.89	664	22.6	2.45	0.933	64.1	595.4	345
350	0.4163	1.027	3.846	2317	4.195	1.954	365	11.09	668	23.0	2.29	0.942	63.2	624.2	350
355	0.5100	1.030	3.180	2304	4.199	1.968	343	11.29	671	23.3	2.14	0.951	62.3	652.3	355
360	0.6209	1.034	2.645	2291	4.203	1.983	324	11.49	674	23.7	2.02	0.960	61.4	697.9	360
365	0.7514	1.038	2.212	2278	4.209	1.999	306	11.69	677	24.1	1.91	0.969	60.5	707.1	365
370	0.9040	1.041	1.861	2265	4.214	2.017	289	11.89	679	24.5	1.80	0.978	59.5	728.7	370
373.15	1.0133	1.044	1.679	2257	4.217	2.029	279	12.02	680	24.8	1.76	0.984	58.9	750.1	373.15
375	1.0815	1.045	1.574	2252	4.220	2.036	274	12.09	681	24.9	1.70	0.987	58.6	761	375
380	1.2869	1.049	1.337	2239	4.226	2.057	260	12.29	683	25.4	1.61	0.999	57.6	788	380
385	1.5233	1.053	1.142	2225	4.232	2.080	248	12.49	685	25.8	1.53	1.004	56.6	814	385
390	1.794	1.058	0.980	2212	4.239	2.104	237	12.69	686	26.3	1.47	1.013	55.6	841	390
400	2.455	1.067	0.731	2183	4.256	2.158	217	13.05	688	27.2	1.34	1.033	53.6	896	400
410	3.302	1.077	0.553	2153	4.278	2.221	200	13.42	688	28.2	1.24	1.054	51.5	952	410
420	4.370	1.088	0.425	2123	4.302	2.291	185	13.79	688	29.8	1.16	1.075	49.4	1010	420
430	5.699	1.099	0.331	2091	4.331	2.369	173	14.14	685	30.4	1.09	1.10	47.2		430

TABLE A.6 *Continued*

Temperature, T (K)	Pressure, p (bar)[b]	Specific Volume (m^3/kg)		Heat of Vaporization, h_{fg} (kJ/kg)	Specific Heat (kJ/kg · K)		Viscosity ($N \cdot s/m^2$)		Thermal Conductivity (W/m · K)		Prandtl Number		Surface Tension, $\sigma_f \cdot 10^3$ (N/m)	Expansion Coefficient, $\beta_f \cdot 10^6$ (K^{-1})	Temperature, T (K)
		$v_f \cdot 10^3$	v_g		$c_{p,f}$	$c_{p,g}$	$\mu_f \cdot 10^6$	$\mu_g \cdot 10^6$	$k_f \cdot 10^3$	$k_g \cdot 10^3$	Pr_f	Pr_g			
440	7.333	1.110	0.261	2059	4.36	2.46	162	14.50	682	31.7	1.04	1.12	45.1		440
450	9.319	1.123	0.208	2024	4.40	2.56	152	14.85	678	33.1	0.99	1.14	42.9		450
460	11.71	1.137	0.167	1989	4.44	2.68	143	15.19	673	34.6	0.95	1.17	40.7		460
470	14.55	1.152	0.136	1951	4.48	2.79	136	15.54	667	36.3	0.92	1.20	38.5		470
480	17.90	1.167	0.111	1912	4.53	2.94	129	15.88	660	38.1	0.89	1.23	36.2		480
490	21.83	1.184	0.0922	1870	4.59	3.10	124	16.23	651	40.1	0.87	1.25	33.9	—	490
500	26.40	1.203	0.0766	1825	4.66	3.27	118	16.59	642	42.3	0.86	1.28	31.6	—	500
510	31.66	1.222	0.0631	1779	4.74	3.47	113	16.95	631	44.7	0.85	1.31	29.3	—	510
520	37.70	1.244	0.0525	1730	4.84	3.70	108	17.33	621	47.5	0.84	1.35	26.9	—	520
530	44.58	1.268	0.0445	1679	4.95	3.96	104	17.72	608	50.6	0.85	1.39	24.5	—	530
540	52.38	1.294	0.0375	1622	5.08	4.27	101	18.1	594	54.0	0.86	1.43	22.1	—	540
550	61.19	1.323	0.0317	1564	5.24	4.64	97	18.6	580	58.3	0.87	1.47	19.7	—	550
560	71.08	1.355	0.0269	1499	5.43	5.09	94	19.1	563	63.7	0.90	1.52	17.3	—	560
570	82.16	1.392	0.0228	1429	5.68	5.67	91	19.7	548	76.7	0.94	1.59	15.0	—	570
580	94.51	1.433	0.0193	1353	6.00	6.40	88	20.4	528	76.7	0.99	1.68	12.8	—	580
590	108.3	1.482	0.0163	1274	6.41	7.35	84	21.5	513	84.1	1.05	1.84	10.5	—	590
600	123.5	1.541	0.0137	1176	7.00	8.75	81	22.7	497	92.9	1.14	2.15	8.4	—	600
610	137.3	1.612	0.0115	1068	7.85	11.1	77	24.1	467	103	1.30	2.60	6.3	—	610
620	159.1	1.705	0.0094	941	9.35	15.4	72	25.9	444	114	1.52	3.46	4.5	—	620
625	169.1	1.778	0.0085	858	10.6	18.3	70	27.0	430	121	1.65	4.20	3.5	—	625
630	179.7	1.856	0.0075	781	12.6	22.1	67	28.0	412	130	2.0	4.8	2.6	—	630
635	190.9	1.935	0.0066	683	16.4	27.6	64	30.0	392	141	2.7	6.0	1.5	—	635
640	202.7	2.075	0.0057	560	26	42	59	32.0	367	155	4.2	9.6	0.8	—	640
645	215.2	2.351	0.0045	361	90	—	54	37.0	331	178	12	26	0.1	—	645
647.3[c]	221.2	3.170	0.0032	0	∞	∞	45	45.0	238	238	∞	∞	0.0	—	647.3[c]

[a]Adapted from Reference 22.
[b]1 bar = 10^5 N/m^2.
[c]Critical temperature.